International Journal of Advanced Biological and Biomedical Research
Available online at http:www.ijabbr.com
Volume 9, Issue 1 (2021) pp. 77-104 **DOI**: 10.22034/ijabbr.2021.45696

*Original Article*

# Theoretical Evaluation of 5, 6-Diaroylisoindoline-1,3-dione as Potential Carcinogenic Kinase PAK1 Inhibitor: DFT Calculation, Molecular Docking Study and ADMET Prediction

**Mohammad Mazharol Hoque, Ajoy Kumer, Md. Sajib Hussen, Md. Wahab Khan***

Department of Chemistry, Bangladesh University of Engineering and Technology, Dhaka-1000, Bangladesh

*Corresponding Author E-mail: mwkhan@chem.buet.ac.bd

Received: 10 July 2020, Revised: 16 September 2020, Accepted: 26 September 2020

**ABSTRACT**

**Background:** The carcinogenic kinase PAK1 (p21-activated kinase 1) is associated with the progression of many disorders, including Alzheimer's disease, various cancers, type-2 diabetes and hypertension. Although few synthetic PAK1 inhibitors and herbal therapeutics, such as propolis and curcumin, are available in the market, a comprehensive remedy of PAK1 related ailments is still not studied in detail. Recently, several phthalimide-metal complexes (viz. Λ-FL172, Λ-FL411, called optically active octahedral ruthenium phthalimide complex) were shown as poor inhibition potency toward PAK1. However, for a full understanding of the inhibition of PAK1 about phthalimide analogues, this study has been designed.

**Methods:** This manuscript presents density functional theory (DFT) based computational approaches of aryl derivatives of phthalimide. The DFT was used to calculate the equilibrium geometries, thermodynamic analysis, dipole moment, polarizability, electrostatic potential map, Mulliken, Hirshfeld, NBO population analysis, frontier molecular orbital contribution, reactivity descriptor, Fukui function analysis of phthalimide derivatives. Molecular docking and ADMET prediction were also performed.

**Result:** The phthalimide derivatives were subjected to molecular docking studies, and binding affinities ranging from -7.3 to -7.7 kcal/mol against PAK1 kinase were determined. The docked ligands demonstrated stronger hydrogen bonding, electrostatic interactions, and hydrophobic interactions with PAK1 kinase. The magnitude of these contacts usually related with bond lengths and attraction forces. The derivatives with an elevated docking score were chosen against ADMET in silico, and they have an excellent oral bioavailability without observed carcinogenesis or mutagenicity affect.

**Conclusion:** These results reveal that these phthalimide derivatives might be potential inhibitors for the protein kinase PAK1.

**Key words:** Isoindoline-1,3-dione, PAK1, Alzheimer's disease, HOMO-LUMO, Fukui function, Molecular Docking, ADMET

## 1. Background

PAK1 is a serine-threonine kinase and member of the p21 activated kinases (PAKs) family. This protein kinase plays a fundamental role in the regulation of cell motility, transmitting a variety of extracellular signals to changes in cytoskeleton organization, cell shape and adhesion which fixes the polarity and physiological activities of cell confined in the tissues [1-3]. These proteins are employed as recipients for the small GTP binding proteins Cdc42 and Rac [4]. Several non-tumorigenic neural disorders have been to involve PAK1 for their development, including Alzheimer's disease (AD), which is the widespread form of dementia, and to date, no effective treatment has been discovered for this age-related diseases [5].

Pathologically, Alzheimer's disease is signposted by prodromal composed of neuritic (seline) plaques containing amyloid-β (Aβ) peptide agglomerates, which instigates neuron cell death. It is recognized that fibrillary AB peptide of 42 amino acid (fAB) stimulates PAK1 through Tiam 1 in a $Ca^{2+}$ dependent manner, which activates RAC/CDC42 [6]. Afterward, PAK1 stimulates LIMK1 by phosphorylation of amino acid residue Thr *508* [7, 8]. LIMK1 contributes in Rac1-mediated actin cytoskeletal reorganization by phosphorylating cofilin [8]. In AD brain, the number of phospho-LIMK-positive neurons is considerably augmented in those areas overstressed by AD pathogenesis (Figure 1). It is worthy to note that blocking the phosphorylation of cofilin by LIMK inhibits the fAB-induced neuronal disintegration [9, 10].

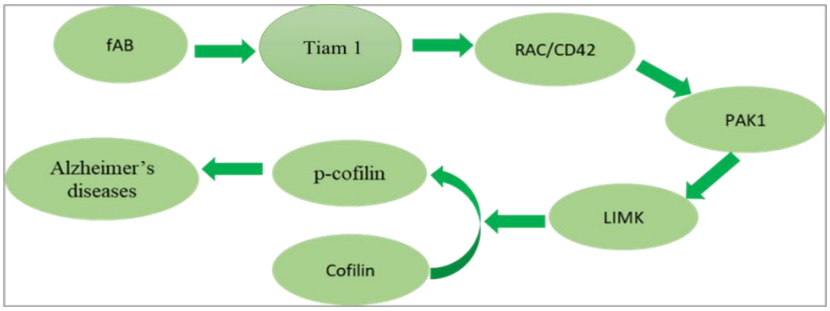


**Figure 1.** PAK1 associated development of Alzheimer's diseases

However, it has been recorded that PAK1 dysregulation is related to multiple tumor types such as breast cancer, whereas the upregulation of this kinase is associated with pancreatic cancer. Various recent studies illustrate that transcriptional modification of fibronectin by PAK1 controls pancreatic tumorigenesis [11, 12]. Therefore, PAK1 has captivated much consideration as a promising oncology target because of their increased expression, activation, and amplification associated with various cancers [13, 14].

Unfortunately, to date, there are no FDA-approved PAK1 blockers available in the market. Several studies demonstrate that some herbal therapeutics, such as propolis and curcumin, and only a few numbers of drugs are available to block PAK1 kinase. Still, they are not fully prescribed as a drug. [15, 16]. Due to -COOH functional group present in herbal therapeutics, cell-permeability is limited in the human body [17]. Therefore, there is an urgent need for efficient discovery and optimization of new PAK1 kinase inhibitors to treat associated cancer. Isoindoline-1,3-dione (Phthalimide) has an inbuilt cyclic imide functionality that allows the compound or its derivatives to

develop as a potential pharmacophore [18]. However, numerous studies demonstrated that the phthalimide-metal complex (viz. Λ-FL172, Λ-FL411) could effectively inhibit PAK1 kinase [19-21].

Screen large numbers of compounds as potential drug candidates through *in vitro* and *in vivo* analysis is becoming gradually more challenging, and computer-aided approaches enable the drug discovery processes to be fast, economical, and resource-efficient. *In silico* approaches can be utilized in all the stages of drug development for the potent and most valuable therapeutic compound with high proficiency [22]. Employing quantum chemistry and computational packages to calculate molecular properties has become a powerful tool because it can investigate a deep perception at the atomistic level [23, 24]. Besides, molecular docking study (MDS) can disclose the interactions and binding energy between drug-like molecules and target macromolecule before animal trail [25]. Density functional theory (DFT) is the most popular method and can compute molecular geometry, internal energy, thermochemistry, electronic properties and different types of intra- or inter-molecular interactions such as hydrogen bonding, halogen bonding [26, 27].

In general, the action of any drug depends on the drug-ligand interaction points. These interactions are governed by molecular structure, frontier molecular orbitals (MOs), and orbitals' energies. Although there are some conception theories by MOs on the drug-ligand interaction, the protein-ligand interaction emerges via only LUMO of the protein and HOMO of the ligand, which is the most acceptable due to its strength and stability for forming drug-protein interaction [28]. Moreover, the amino acids or atoms positioned both on the LUMOs of a protein, and surface pocket of a protein performs as activity atoms of the protein. Eventually, these residues or atoms serve as the ligand-binding location [28]. However, HOMO and LUMO energy gap of drug molecule can be used to estimate the chemical descriptors such as chemical potential (μ), electronegativity (χ), hardness (η), and softness (σ) of a drug molecule. Moreover, the Fukui Function is used to recognize the most reactive sites for the electrophilic, nucleophilic, or radical attack within the molecule [29].

Another essential feature of a drug molecule's electronic structure is the molecular electrostatic potential (MEP) map calculated on the isolated chemical system, which can be used to forecast reactivity indexes such as electrophilic sites and nucleophilic attacks [30]. Moreover, the MEP is mainly a useful tool that provides insights into the intermolecular association and molecular properties of small molecules and the action of a drug molecule with the target protein. Hydrogen-bonding interactions are vital in drug action, and it often regulates drug solubility, partitioning, and receptor binding [31]. As the hydrogen-bonding is formed for the electrostatic interactions between drug and protein, it could be used to measure the binding affinity.

Dipole moments within drug molecules are vital for their interaction with the macromolecules within cell. Significant dipole moments facilitate stronger dipolar interaction with the protein or receptor. It also gives a sign of how likely the drug is to be disintegrated by the reactants with an attraction towards the positive and negative charges[32]. However, the polarizability of a drug molecule plays a central role in describing the structural orientation and thermodynamics. Moreover, it is also advantageous in pharmacology to derive Quantitative Structural Activity Relationships (QSARs) and drug design [33].

This manuscript presents the theoretical study of isoindoline-1, 3-dione, and its aroyl derivatives as potential PAK1

kinase inhibitors. There are a few synthetic approaches, palladium-catalyzed oxidative -C–H aroylation, ZnI-catalyzed Diels–Alder reaction, and Fe-catalyzed oxidative radical cyclization for the synthesis of aryl derivatives of the aromatic substrate [34-37]. Hence, this study is designed for a theoretical investigation on the new molecules derived from isoindoline-1, 3-dione, and its aryl derivatives. DFT method was used to optimize the equilibrium geometry of compounds (PH 1-5) (Figure 2; Table 1-5). Thermodynamic properties and the Frontier MOs, such as the HOMO and LUMO, were analyzed in detail. The HOMO-LUMO energy gap was also calculated to predict global chemical potential(μ), electronegativity (χ), hardness (η) and softness (σ) for the studied compounds [38]. The Fukui function was also calculated to predict the local reactivity these compounds. The Structure-based Virtual Screening (VS) using Auto Dock Vina was also employed in this study. The docking results were investigated using Accelrys Discovery Studio 4.1 to revel nonbonding interactions between the ligands PH **1-5** and PAK1 kinase (PDB ID: 4DAW). These compounds were exposed to ADMET (absorption, distribution, metabolism, excretion, and toxicity) prediction to reveal their pharmacokinetic properties.

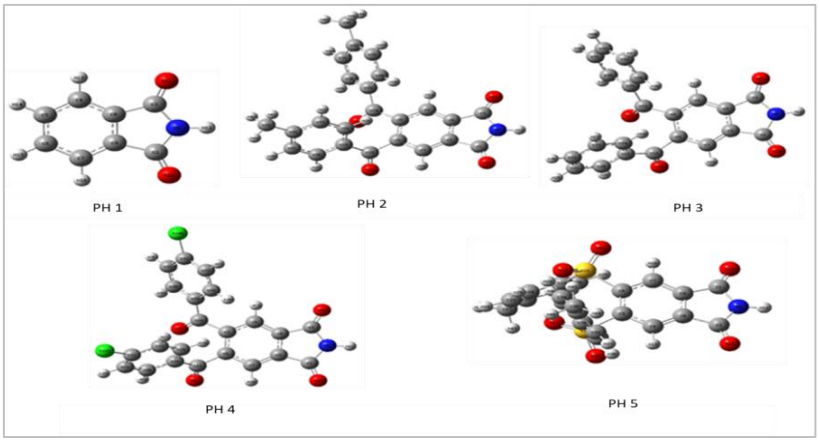


**Figure 2**. Optimized structure of PH 1-5

**Table 1.** Bond distance (Å), Bond angle (°) and Dihedral angle (°) of PH 1

| Atom | Bond Atom | Bond length(Å) | Angle atom | Bond angle (°) | 2nd angle atom | 2nd angle (°) | 2nd angle type |
|---|---|---|---|---|---|---|---|
| C(1) | | | | | | | |
| N(2) | C(1) | 1.4034 | | | | | |
| C(3) | N(2) | 1.4034 | C(1) | 113.5484 | | | |
| H(12) | N(2) | 1.0110 | C(1) | 123.2258 | C(3) | 123.2258 | Pro-R |
| C(8) | C(3) | 1.4954 | N(2) | 104.7061 | C(1) | 0.0000 | Dihedral |
| O(11) | C(3) | 1.2128 | N(2) | 126.0080 | C(8) | 129.2859 | Pro-R |
| C(4) | C(8) | 1.3875 | C(3) | 129.9782 | N(2) | 180.0000 | Dihedral |
| C(9) | C(8) | 1.3980 | C(3) | 108.5198 | C(4) | 121.5020 | Pro-R |
| C(7) | C(9) | 1.3875 | C(1) | 129.9782 | C(8) | 121.5020 | Pro-R |
| O(10) | C(1) | 1.2128 | N(2) | 126.0080 | C(9) | 129.2859 | Pro-R |
| C(5) | C(4) | 1.4010 | C(8) | 117.4290 | C(3) | 180.0000 | Dihedral |
| H(13) | C(4) | 1.0851 | C(5) | 121.7026 | C(8) | 120.8683 | Pro-R |
| C(6) | C(7) | 1.4010 | C(9) | 117.4290 | C(1) | 180.0000 | Dihedral |
| H(14) | C(5) | 1.0862 | C(4) | 119.6049 | C(6) | 119.3261 | Pro-R |
| H(15) | C(6) | 1.0862 | C(5) | 119.3261 | C(7) | 119.6049 | Pro-R |
| H(16) | C(7) | 1.0851 | C(6) | 121.7026 | C(9) | 120.8683 | Pro-R |

**Table 2.** Bond distance (Å), Bond angle (°) and Dihedral angle (°) of PH 2

| Atom | Bond Atom | Bond length(Å) | Angle atom | Bond angle (°) | 2nd angle atom | 2nd angle (°) | 2nd angle type |
|---|---|---|---|---|---|---|---|
| C(1) | | | | | | | |
| N(2) | C(1) | 1.4037 | | | | | |
| C(3) | N(2) | 1.4026 | C(1) | 113.6697 | | | |
| H(12) | N(2) | 1.0116 | C(1) | 123.0982 | C(3) | 123.2321 | Pro-S |
| C(8) | C(3) | 1.4951 | N(2) | 104.5744 | C(1) | -0.0131 | Dihedral |
| O(11) | C(3) | 1.2126 | N(2) | 126.1279 | C(8) | 129.2972 | Pro-S |
| C(4) | C(8) | 1.3851 | C(3) | 130.0410 | N(2) | -179.6129 | Dihedral |
| C(9) | C(8) | 1.3953 | C(3) | 108.7053 | C(4) | 121.2517 | Pro-S |
| C(7) | C(9) | 1.3850 | C(1) | 130.2534 | C(8) | 121.2669 | Pro-S |
| O(10) | C(1) | 1.2118 | N(2) | 126.0860 | C(9) | 129.3365 | Pro-R |
| C(5) | C(4) | 1.4070 | C(8) | 118.5057 | C(3) | 179.7834 | Dihedral |
| H(13) | C(4) | 1.0853 | C(5) | 121.0024 | C(8) | 120.4687 | Pro-S |
| C(6) | C(7) | 1.4041 | C(9) | 118.5015 | C(1) | 179.7816 | Dihedral |
| C(14) | C(5) | 1.5099 | C(4) | 119.9059 | C(6) | 119.4780 | Pro-R |
| C(15) | C(6) | 1.5192 | C(5) | 123.7830 | C(7) | 115.8303 | Pro-R |
| H(16) | C(7) | 1.0856 | C(6) | 120.1843 | C(9) | 121.3125 | Pro-R |
| C(19) | C(15) | 1.4901 | C(6) | 120.2545 | C(5) | -59.9066 | Dihedral |
| O(18) | C(15) | 1.2224 | C(6) | 117.7727 | C(19) | 121.7495 | Pro-R |
| C(20) | C(19) | 1.4040 | C(15) | 118.1934 | C(6) | 168.8880 | Dihedral |
| C(24) | C(19) | 1.4003 | C(15) | 122.9099 | C(20) | 118.8204 | Pro-S |
| C(21) | C(20) | 1.3874 | C(19) | 120.4515 | C(15) | 177.9367 | Dihedral |
| H(25) | C(20) | 1.0847 | C(19) | 118.4882 | C(21) | 121.0602 | Pro-S |
| C(22) | C(21) | 1.4054 | C(20) | 121.0920 | C(19) | -0.6967 | Dihedral |
| H(26) | C(21) | 1.0885 | C(20) | 119.6156 | C(22) | 119.2923 | Pro-R |
| C(23) | C(24) | 1.3939 | C(19) | 120.4166 | C(15) | -177.1932 | Dihedral |
| C(39) | C(22) | 1.5100 | C(21) | 120.6301 | C(23) | 121.2040 | Pro-S |
| H(27) | C(23) | 1.0877 | C(22) | 119.4357 | C(24) | 119.5189 | Pro-R |
| H(28) | C(24) | 1.0861 | C(19) | 120.2203 | C(23) | 119.3483 | Pro-S |
| C(29) | C(14) | 1.4915 | C(5) | 120.4583 | C(4) | -41.7353 | Dihedral |
| O(17) | C(14) | 1.2251 | C(5) | 118.5086 | C(29) | 121.0161 | Pro-S |
| C(30) | C(29) | 1.4057 | C(14) | 117.8093 | C(5) | 160.8020 | Dihedral |
| C(34) | C(29) | 1.4026 | C(14) | 123.5027 | C(30) | 118.6104 | Pro-S |
| C(31) | C(30) | 1.3889 | C(29) | 120.5545 | C(14) | 178.1261 | Dihedral |
| H(35) | C(30) | 1.0845 | C(29) | 118.4733 | C(31) | 120.9719 | Pro-R |
| C(32) | C(31) | 1.4051 | C(30) | 121.0417 | C(29) | -0.8216 | Dihedral |
| H(36) | C(31) | 1.0870 | C(30) | 119.5467 | C(32) | 119.4110 | Pro-R |
| C(33) | C(34) | 1.3936 | C(29) | 120.4898 | C(14) | -177.2222 | Dihedral |
| C(40) | C(32) | 1.5091 | C(31) | 120.6400 | C(33) | 121.1544 | Pro-S |
| H(37) | C(33) | 1.0877 | C(32) | 119.4855 | C(34) | 119.4276 | Pro-S |
| H(38) | C(34) | 1.0853 | C(29) | 120.2603 | C(33) | 119.2349 | Pro-S |
| H(41) | C(39) | 1.0948 | C(22) | 111.5683 | C(21) | 167.6018 | Dihedral |
| H(42) | C(39) | 1.0978 | C(22) | 111.0504 | H(41) | 107.5618 | Pro-S |
| H(43) | C(39) | 1.0960 | C(22) | 111.3918 | H(41) | 108.0233 | Pro-R |
| H(44) | C(40) | 1.0977 | C(32) | 110.9735 | C(31) | -77.0664 | Dihedral |
| H(45) | C(40) | 1.0956 | C(32) | 111.4306 | H(44) | 107.0320 | Pro-S |
| H(46) | C(40) | 1.0944 | C(32) | 111.5804 | H(44) | 107.5141 | Pro-R |

**Table 3.** Bond distance (Å), Bond angle (°) and Dihedral angle (°) of PH 3

| Atom | Bond Atom | Bond length(Å) | Angle atom | Bond angle (°) | 2nd angle atom | 2nd angle (°) | 2nd angle type |
|---|---|---|---|---|---|---|---|
| C(1) | | | | | | | |
| N(2) | C(1) | 1.4036 | | | | | |
| C(3) | N(2) | 1.4029 | C(1) | 113.7342 | | | |
| H(12) | N(2) | 1.0120 | C(1) | 123.1552 | C(3) | 123.1106 | Pro-R |
| C(8) | C(3) | 1.4965 | N(2) | 104.5207 | C(1) | 0.0534 | Dihedral |
| O(11) | C(3) | 1.2117 | N(2) | 126.2612 | C(8) | 129.2176 | Pro-S |
| C(4) | C(8) | 1.3849 | C(3) | 129.9962 | N(2) | -179.6365 | Dihedral |
| C(9) | C(8) | 1.3951 | C(3) | 108.6712 | C(4) | 121.3306 | Pro-S |
| C(7) | C(9) | 1.3858 | C(1) | 130.1992 | C(8) | 121.2608 | Pro-S |
| O(10) | C(1) | 1.2111 | N(2) | 126.1074 | C(9) | 129.3511 | Pro-R |
| C(5) | C(4) | 1.4076 | C(8) | 118.4080 | C(3) | 179.7416 | Dihedral |
| H(13) | C(4) | 1.0849 | C(5) | 121.0555 | C(8) | 120.5110 | Pro-S |
| C(6) | C(7) | 1.4038 | C(9) | 118.4218 | C(1) | 179.8839 | Dihedral |
| C(14) | C(5) | 1.5087 | C(4) | 119.9324 | C(6) | 119.4229 | Pro-R |
| C(15) | C(6) | 1.5194 | C(5) | 123.7198 | C(7) | 115.8247 | Pro-R |
| H(16) | C(7) | 1.0853 | C(6) | 120.2550 | C(9) | 121.3208 | Pro-R |
| C(19) | C(15) | 1.4935 | C(6) | 120.2578 | C(5) | -59.8865 | Dihedral |
| O(18) | C(15) | 1.2209 | C(6) | 117.9113 | C(19) | 121.6001 | Pro-R |
| C(20) | C(19) | 1.4030 | C(15) | 117.9632 | C(6) | 167.8760 | Dihedral |
| C(24) | C(19) | 1.4027 | C(15) | 122.5471 | C(20) | 119.4191 | Pro-S |
| C(21) | C(20) | 1.3908 | C(19) | 120.2302 | C(15) | 178.0342 | Dihedral |
| H(25) | C(20) | 1.0847 | C(19) | 118.4671 | C(21) | 121.3022 | Pro-S |
| C(22) | C(21) | 1.3990 | C(20) | 120.1053 | C(19) | -0.8046 | Dihedral |
| H(26) | C(21) | 1.0869 | C(20) | 119.9202 | C(22) | 119.9744 | Pro-R |
| C(23) | C(24) | 1.3950 | C(19) | 120.2232 | C(15) | -177.3012 | Dihedral |
| H(27) | C(23) | 1.0861 | C(22) | 120.1982 | C(24) | 119.7838 | Pro-R |
| H(28) | C(24) | 1.0861 | C(19) | 120.1315 | C(23) | 119.6343 | Pro-S |
| H(39) | C(22) | 1.0865 | C(21) | 120.0278 | C(23) | 119.9760 | Pro-R |
| C(29) | C(14) | 1.4943 | C(5) | 120.5865 | C(4) | -40.6769 | Dihedral |
| O(17) | C(14) | 1.2254 | C(5) | 118.5855 | C(29) | 120.8116 | Pro-S |
| C(30) | C(29) | 1.4054 | C(14) | 117.6162 | C(5) | 159.5001 | Dihedral |
| C(34) | C(29) | 1.4047 | C(14) | 123.1277 | C(30) | 119.1778 | Pro-S |
| C(31) | C(30) | 1.3905 | C(29) | 120.4087 | C(14) | 178.1339 | Dihedral |
| H(35) | C(30) | 1.0848 | C(29) | 118.4541 | C(31) | 121.1372 | Pro-R |
| C(32) | C(31) | 1.3988 | C(30) | 119.9893 | C(29) | -0.9351 | Dihedral |
| H(36) | C(31) | 1.0856 | C(30) | 119.9386 | C(32) | 120.0719 | Pro-R |
| C(33) | C(34) | 1.3937 | C(29) | 120.2983 | C(14) | -177.2735 | Dihedral |
| H(37) | C(33) | 1.0867 | C(32) | 120.1759 | C(34) | 119.7787 | Pro-R |
| H(38) | C(34) | 1.0857 | C(29) | 120.1400 | C(33) | 119.5523 | Pro-S |
| H(40) | C(32) | 1.0868 | C(31) | 120.0072 | C(33) | 119.9245 | Pro- R |

**Table 4. Bond distance (Å), Bond angle (°) and Dihedral angle (°)** of PH 4

| Atom | Bond Atom | Bond length(Å) | Angle atom | Bond angle (°) | 2nd angle atom | 2nd angle (°) | 2nd angle type |
|---|---|---|---|---|---|---|---|
| C(1) | | | | | | | |
| N(2) | C(1) | 1.4032 | | | | | |
| C(3) | N(2) | 1.4021 | C(1) | 113.7604 | | | |
| H(12) | N(2) | 1.0118 | C(1) | 123.1189 | C(3) | 123.1206 | Pro-R |
| C(8) | C(3) | 1.4971 | N(2) | 104.5268 | C(1) | 0.0655 | Dihedral |
| O(11) | C(3) | 1.2115 | N(2) | 126.3443 | C(8) | 129.1283 | Pro-S |
| C(4) | C(8) | 1.3845 | C(3) | 129.9975 | N(2) | -179.5984 | Dihedral |
| C(9) | C(8) | 1.3947 | C(3) | 108.6879 | C(4) | 121.3120 | Pro-S |
| C(7) | C(9) | 1.3850 | C(1) | 130.1884 | C(8) | 121.3220 | Pro-S |
| O(10) | C(1) | 1.2114 | N(2) | 126.1993 | C(9) | 129.2579 | Pro-R |
| C(5) | C(4) | 1.4081 | C(8) | 118.4143 | C(3) | 179.7746 | Dihedral |
| H(13) | C(4) | 1.0845 | C(5) | 121.1222 | C(8) | 120.4344 | Pro-S |
| C(6) | C(7) | 1.4040 | C(9) | 118.3867 | C(1) | 179.8464 | Dihedral |
| C(14) | C(5) | 1.5077 | C(4) | 120.0593 | C(6) | 119.3195 | Pro-R |
| C(15) | C(6) | 1.5190 | C(5) | 123.7205 | C(7) | 115.7999 | Pro-R |
| H(16) | C(7) | 1.0856 | C(6) | 120.2575 | C(9) | 121.3539 | Pro-R |
| C(19) | C(15) | 1.4935 | C(6) | 120.2467 | C(5) | -60.1040 | Dihedral |
| O(18) | C(15) | 1.2207 | C(6) | 118.0767 | C(19) | 121.4518 | Pro-R |
| C(20) | C(19) | 1.4034 | C(15) | 117.9556 | C(6) | 168.0329 | Dihedral |
| C(24) | C(19) | 1.4007 | C(15) | 122.8338 | C(20) | 119.1419 | Pro-S |
| C(21) | C(20) | 1.3899 | C(19) | 120.7462 | C(15) | 178.1162 | Dihedral |
| H(25) | C(20) | 1.0851 | C(19) | 118.6144 | C(21) | 120.6389 | Pro-S |
| C(22) | C(21) | 1.3981 | C(20) | 119.0434 | C(19) | -0.8482 | Dihedral |
| H(26) | C(21) | 1.0851 | C(20) | 120.9319 | C(22) | 120.0246 | Pro-R |
| C(23) | C(24) | 1.3931 | C(19) | 120.7606 | C(15) | -177.3331 | Dihedral |
| H(27) | C(23) | 1.0848 | C(22) | 120.0488 | C(24) | 120.9227 | Pro-R |
| H(28) | C(24) | 1.0865 | C(19) | 120.2648 | C(23) | 118.9623 | Pro-S |
| Cl(39) | C(22) | 1.7539 | C(21) | 119.3405 | C(23) | 119.3888 | Pro-R |
| C(29) | C(14) | 1.4945 | C(5) | 120.6483 | C(4) | -40.5656 | Dihedral |
| O(17) | C(14) | 1.2241 | C(5) | 118.7548 | C(29) | 120.5882 | Pro-S |
| C(30) | C(29) | 1.4048 | C(14) | 117.5753 | C(5) | 160.5102 | Dihedral |
| C(34) | C(29) | 1.4031 | C(14) | 123.4045 | C(30) | 118.9339 | Pro-S |
| C(31) | C(30) | 1.3891 | C(29) | 120.8963 | C(14) | 178.0030 | Dihedral |
| H(35) | C(30) | 1.0849 | C(29) | 118.5809 | C(31) | 120.5227 | Pro-R |
| C(32) | C(31) | 1.3975 | C(30) | 119.0641 | C(29) | -1.0180 | Dihedral |
| H(36) | C(31) | 1.0847 | C(30) | 120.8744 | C(32) | 120.0608 | Pro-R |
| C(33) | C(34) | 1.3934 | C(29) | 120.7526 | C(14) | -177.1064 | Dihedral |
| H(37) | C(33) | 1.0850 | C(32) | 120.1247 | C(34) | 120.7634 | Pro-R |
| H(38) | C(34) | 1.0851 | C(29) | 120.3957 | C(33) | 118.8411 | Pro-S |
| Cl(40) | C(32) | 1.7513 | C(31) | 119.3858 | C(33) | 119.3847 | Pro-R |

**Table 5.** Bond distance (Å), Bond angle (°) and Dihedral angle (°) of PH 5

| Atom | Bond Atom | Bond length(Å) | Angle atom | Bond angle (°) | 2nd angle atom | 2nd angle (°) | 2nd angle type |
|---|---|---|---|---|---|---|---|
| C(1) | | | | | | | |
| N(2) | C(1) | 1.4032 | | | | | |
| C(3) | N(2) | 1.4021 | C(1) | 113.7604 | | | |
| H(12) | N(2) | 1.0118 | C(1) | 123.1189 | C(3) | 123.1206 | Pro-R |
| C(8) | C(3) | 1.4971 | N(2) | 104.5268 | C(1) | 0.0655 | Dihedral |
| O(11) | C(3) | 1.2115 | N(2) | 126.3443 | C(8) | 129.1283 | Pro-S |
| C(4) | C(8) | 1.3845 | C(3) | 129.9975 | N(2) | -179.5984 | Dihedral |
| C(9) | C(8) | 1.3947 | C(3) | 108.6879 | C(4) | 121.3120 | Pro-S |
| C(7) | C(9) | 1.3850 | C(1) | 130.1884 | C(8) | 121.3220 | Pro-S |
| O(10) | C(1) | 1.2114 | N(2) | 126.1993 | C(9) | 129.2579 | Pro-R |
| C(5) | C(4) | 1.4081 | C(8) | 118.4143 | C(3) | 179.7746 | Dihedral |
| H(13) | C(4) | 1.0845 | C(5) | 121.1222 | C(8) | 120.4344 | Pro-S |
| C(6) | C(7) | 1.4040 | C(9) | 118.3867 | C(1) | 179.8464 | Dihedral |
| C(14) | C(5) | 1.5077 | C(4) | 120.0593 | C(6) | 119.3195 | Pro-R |
| C(15) | C(6) | 1.5190 | C(5) | 123.7205 | C(7) | 115.7999 | Pro-R |
| H(16) | C(7) | 1.0856 | C(6) | 120.2575 | C(9) | 121.3539 | Pro-R |
| C(19) | C(15) | 1.4935 | C(6) | 120.2467 | C(5) | -60.1040 | Dihedral |
| O(18) | C(15) | 1.2207 | C(6) | 118.0767 | C(19) | 121.4518 | Pro-R |
| C(20) | C(19) | 1.4034 | C(15) | 117.9556 | C(6) | 168.0329 | Dihedral |
| C(24) | C(19) | 1.4007 | C(15) | 122.8338 | C(20) | 119.1419 | Pro-S |
| C(21) | C(20) | 1.3899 | C(19) | 120.7462 | C(15) | 178.1162 | Dihedral |
| H(25) | C(20) | 1.0851 | C(19) | 118.6144 | C(21) | 120.6389 | Pro-S |
| C(22) | C(21) | 1.3981 | C(20) | 119.0434 | C(19) | -0.8482 | Dihedral |
| H(26) | C(21) | 1.0851 | C(20) | 120.9319 | C(22) | 120.0246 | Pro-R |
| C(23) | C(24) | 1.3931 | C(19) | 120.7606 | C(15) | -177.3331 | Dihedral |
| H(27) | C(23) | 1.0848 | C(22) | 120.0488 | C(24) | 120.9227 | Pro-R |
| H(28) | C(24) | 1.0865 | C(19) | 120.2648 | C(23) | 118.9623 | Pro-S |
| Cl(39) | C(22) | 1.7539 | C(21) | 119.3405 | C(23) | 119.3888 | Pro-R |
| C(29) | C(14) | 1.4945 | C(5) | 120.6483 | C(4) | -40.5656 | Dihedral |
| O(17) | C(14) | 1.2241 | C(5) | 118.7548 | C(29) | 120.5882 | Pro-S |
| C(30) | C(29) | 1.4048 | C(14) | 117.5753 | C(5) | 160.5102 | Dihedral |
| C(34) | C(29) | 1.4031 | C(14) | 123.4045 | C(30) | 118.9339 | Pro-S |
| C(31) | C(30) | 1.3891 | C(29) | 120.8963 | C(14) | 178.0030 | Dihedral |
| H(35) | C(30) | 1.0849 | C(29) | 118.5809 | C(31) | 120.5227 | Pro-R |
| C(32) | C(31) | 1.3975 | C(30) | 119.0641 | C(29) | -1.0180 | Dihedral |
| H(36) | C(31) | 1.0847 | C(30) | 120.8744 | C(32) | 120.0608 | Pro-R |
| C(33) | C(34) | 1.3934 | C(29) | 120.7526 | C(14) | -177.1064 | Dihedral |
| H(37) | C(33) | 1.0850 | C(32) | 120.1247 | C(34) | 120.7634 | Pro-R |
| H(38) | C(34) | 1.0851 | C(29) | 120.3957 | C(33) | 118.8411 | Pro-S |
| Cl(40) | C(32) | 1.7513 | C(31) | 119.3858 | C(33) | 119.3847 | Pro-R |

## 2. Computational details

### 2.1. Geometry optimization, thermodynamic and electronic properties computed using quantum mechanical calculations

All calculations were carried out using Gaussian 09 software package [39] employing DFT methods. The calculated equilibrium geometry, Gibbs free energy, internal electronic energy, entropy, dipole moment, and polarizability, frontier MO calculation of PH **1-5** were investigated using the Becke, three parameters, Lee-Yang-Parr (B3LYP) correlation functional coupled with the basis set 6-31G(d) and 6-31G(d, p) [40]. The finite difference approximation of

the partial derivatives $\left(\frac{\partial E}{\partial N}\right)_v$ gives the chemical potential (μ) and electronegativity, χ defined within DFT that is given (i) by Mulliken [41].

$$-\mu = \chi = \frac{1}{2}[I + A] \quad \text{(i)}$$

Where I= ionization potential and A= electronegativity. According to Molecular Orbital Theory (MOT), I and A can be approximated from HOMO and LUMO's negative energies. In this framework, the electronegativity is the negative of HOMO- LUMO energy average and can be written as [42].

$$-\chi = \mu = \frac{1}{2}[\varepsilon HOMO + \varepsilon LUMO] \quad \text{(ii)}$$

(η ) [42] of a chemical is defined as half of the energy gap between HOMO and LUMO, and softness(σ) is defined as the inverse of hardness. Hardness of a molecule has the ability to help predict chemical behavior [43]. According to Koopmans' theorem [44], hardness(η ) and softness (σ) are given by equation (iii). and (iv), and Parr et al. [45] defined global electrophilicity ($\omega$) as equations (v), respectively.

$$\eta = \frac{1}{2}[\varepsilon LUMO - \varepsilon HOMO] \quad \text{(iii)}$$

$$\sigma = \frac{1}{\eta} \quad \text{(iv)}$$

$$\omega = \frac{\mu^2}{2} \quad \text{(v)}$$

However, the polarizability is defined as the linear response of a molecular electronic distribution to an external electric field. The polarizability (α) is given by the equation (vi) [46-48].

$$\alpha = \frac{1}{3}\left(\alpha_{xx} + \alpha_{yy} + \alpha_z\alpha_z\right) \quad \text{(vi)}$$

Here x, y and z are Cartesians axis and α is polarizable tensor.

## 2.2. Fukui Function analysis

Fukui Function indicates the tendency of the electronic density to deform at a given site upon the acceptance or donation of electrons [49, 50]. This index is presented to recognize the most reactive sites for the electrophilic, nucleophilic, or radical attack within the molecule. The condensed Fukui Function [51] for the $k^{th}$ atom site in a molecule is given by

$$f_k^+ = [q_k(N+1) - q_k(N)]$$

for atom k as an electrophile

$$f_k^- = [q_k(N) - q_k(N-1)]$$

for atom k as a nucleophile

$$f_k^0 = \frac{1}{2}[q_k(N+1) - q_k(N-1)]$$

for atom k as a radical

Here, $q_k(N)$ is the electron population on atom k. q is the electron population on the $k^{th}$ atom site. In molecule local softness ($s_k^+, s_k^-$) and local electrophilicity ($\omega_k^+$, $\omega_k^-$) are estimated utilizing the Fukui function ($f_k^+, f_k^-$), global softness(S) and global electrophilicity ($\omega$) using the following equations.

$$s_k^+ = Sf_k^+;\ s_k^- = Sf_k^- \quad \text{(vii)}$$

$$\omega_k^+ = \omega f_k^+;\ \omega_k^- = \omega f_k^- \quad \text{(viii)}$$

## 2.3. Preparation of Ligands and Target protein (PAK1) structure for Docking

For docking analysis, ligands PH 1-5 were subjected to quantum mechanical treatment for geometry optimization and frequency calculation employing B3LYP/6-31G (d) and 6-31G (d, p) level of theory. The main reason for selecting B3LYP/6-31G (d) is explained as follows: B3LYP/6-31G (d) method was used to optimize the ligands (PH 1 - PH 5) (Table 1-5), which resulted in a particular bond length, bond angle and dihedral angle for each of the ligands. These structural parameters are found to optimal for the best docking score and binding postures with PAK1. Adding one p polarization term on hydrogen atoms of all the ligands, i.e., using a basis set 6-31G (d, p), brings some changes to the structural

parameters. Moreover, other physiochemical parameters, for instance, dipole moment and polarizability, realizes a substantial change, as it is evident from Table 7. Finally, the resulting geometry produces poor docking scores and binding postures. A similar effect is observed when the diffusion term is added in the basis set. Crystal structure of PAK1 kinase (PDB ID: 4DAW, resolution, 2 Å) was obtained from RCSB PDB (https://www.rcsb.org/structure/4daw) [52]. The co-crystalized ligand, water molecule, and other heteroatoms were removed from PAK1 structure using the PyMol Molecular Graphics System software[53]. Subsequently, Swiss-PDB viewer software packages (version 4.1.0)[54] was used for energy minimization and to resolve improper bond order, missing amino acids, and hydrogen(s). The highest binding pocket area, the volume of the active binding site, and the amino acid residues present in the active site and their residue number were calculated using CASTp [55]. The ligands structure and protein structure were saved in PDBQT file format by Auto dock Vina Software (version 1.1.2) [56] for docking analysis.

**Table 6.** Molecular formula and IUPAC name of ligands PH 1 - PH 5

| Abbreviation of Ligand | Molecular Formula | IUPAC Name |
|---|---|---|
| PH 1 | $C_8H_5NO_2$ | Isoindoline-1, 3-dione |
| PH 2 | $C_{24}H_{17}NO_4$ | 5, 6-bis(4-methylbenzoyl) isoindoline-1, 3-dione |
| PH 3 | $C_{22}H_{13}NO_4$ | 5, 6-dibenzoylisoindoline-1, 3-dione |
| PH 4 | $C_{22}H_{11}Cl_2NO_4$ | 5, 6-bis(4-chlorobenzoyl) isoindoline-1, 3-dione |
| PH 5 | $C_{22}H_{17}NO_8S_2$ | di-p-tolyl-1, 3-dioxoisoindoline-5, 6-disulfonate |

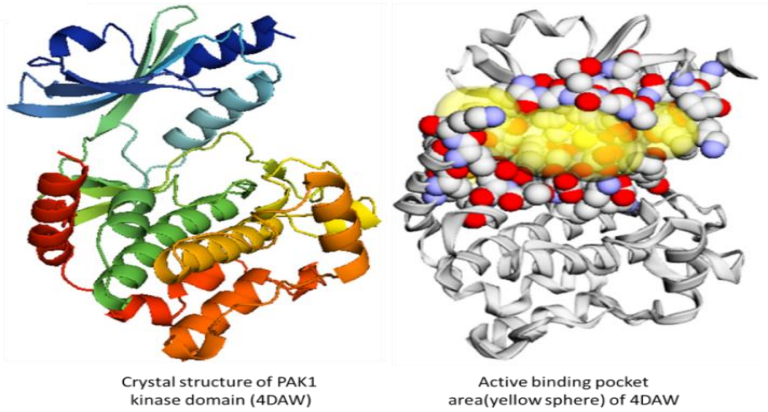


**Figure 3**. Crystal structure (left) and active binding pocket area (right) of PAK1 Kinase domain (PDB ID: 4DAW)

## 2.4. Analysis and Visualization of Docking Results

The CASTp (http://cast.engr.uic.edu) is a virtual program used to analyze 4DAW kinase's active binding pocket area and volume. The calculated values are 719.9 Å2 and 826.7 Å3, respectively. Auto Dock Vina docking software was employed to conduct the docking study. To perform the docking studies of compounds 1-5 against PAK1, the center of the grid box was set at X = 10.8785, Y = 24.795, Z = 13.6769, and the dimension

of the grid box was made into 25, 25 and 25 Å in the x, y and z-direction, respectively by default. However, to maximize the search place, the grid box size was made larger enough by selecting the pop-up menu to the maximum. The highest binding free energy conformer with the corresponding protein was investigated using Accelrys Discovery Studio 4.1[57].

### 2.5. Pharmacokinetic Parameters

To guess the indicators related to organic compounds, absorption, distribution, metabolism, excretion, and toxicity parameters for phthalimide and its derivatives were calculated employing admetSAR and SwissADME [58, 59] software. For this purpose, the Simplified Molecular Input Line Entry System (SMILES) was used during the generation process.

## 3. Results and discussions

### 3.1. Geometry optimization

The optimized geometries of isoindoline-1, 3-dione, and its derivatives PH 1-5 were obtained at B3LYP functional coupled with the 6-31G (d) and 6-31G (d, p) basis sets. The optimized structures are given in Figure 2, and the bond distances (Å), bond angles (°), and dihedral angles (°) of PH 1-5 are given in the Tables 1–5. In this study, the estimated structural parameters like bond distances, bond angle, and dihedral angle of phthalimide display consistency with the reported crystal structure of phthalimide determined by the X-ray diffraction technique [60]. For example, the estimated bond distances of N2-C1 and N2-C3 are equal, with a value of 1.403 Å, following the experimental data (1.388 Å). Similarly, the calculated structural parameters for compounds PH 2-5 show resemblances with the optimized structure of phthalimide and have been employed for further analysis.

This study predicts that PH 1 has the Gibbs free energy -513.135 Hartrees, and the derivatives of PH 2-PH 5 are perceived to have more negative Gibbs free energy [Table 7]. It is recognized that the more negative ΔG of a chemical system leads to greater stability. From this viewpoint, it could be inferred that all derivatives PH 2-5 are thermodynamically more stable than PH 1, predicting the highest stability of derivative PH 5. The increased entropy of a chemical system signpost is a more unsystematic distribution of energy. Hence, the system develops a more stable state when its energy is spread out in a more chaotic state.

However, from DFT computations, it is estimated that PH 1 possesses a dipole moment of 2.796 Debye. This value is in accordance with the recorded value of 2.910 Debye [61]. On the other hand, PH 2 and PH 3 exhibit significantly increased dipole moment values of 6.67 and 5.631 Debye. Several studies show that increased dipole moments enable highly-favored hydrogen bonding and non-bond interaction in the macromolecule-ligand complex [10, 62]. This postulation is found to reflect in the complex of PAK1 with the ligand PH 2 and PH 3, exhibiting stronger hydrogen bonding in contrast to ligand PH 1. On the other hand, the polarizability of a drug molecule governs some crucial issues on the drug action. For instance, the octanol-water partition coefficient (LogP), which forecasts how rapidly an organic toxicant can be shifted from water to lipid, is estimated as polarizability control [62]. This calculation reveals that PH 4 elucidates the highest polarizability (4.459×10-39 C2 m2 J-1) among the non-carcinogen's derivatives, and hence, it shows the highest octanol-water partition coefficient LogP (4.66) in ADMET prediction.

**Table 7.** Gibbs free energy (ΔG, Hartree), Entropy (S, a. u), Heat Capacity ($C_v$, Cal/Mol-Kelvin), Dipole moment (μ, Debye) and Polarizability (α, $10^{-39}$ in $C^3m^3J^{-1}$) for PH 1-5 calculated at B3LYP/6-31G (d) and 6-31G (d, p) level theories

| Entry | Basis set | Compounds | | | | |
|---|---|---|---|---|---|---|
| | | PH 1 | PH 2 | PH 3 | PH 4 | PH 5 |
| Gibbs free energy (ΔG) (Hartree/mol) | 6-31G (d) | -513.135 | -1280.141 | -1201.849 | -2121.039 | -2150.949 |
| | 6-31G (d, p) | -513.103 | -1280.514 | -1201.871 | -2121.059 | -2150.977 |
| Entropy(S) (a. u) | 6-31G (d) | 30.929 | 92.649 | 82.272 | 89.991 | 105.357 |
| | 6-31G (d, p) | 30.961 | 94.511 | 82.34 | 90.054 | 105.503 |
| Heat Capacity (Cv) (Cal/Mol-Kelvin) | 6-31G (d) | 87.654 | 176.507 | 156.871 | 171.484 | 192.48 |
| | 6-31G (d, p) | 87.648 | 178.601 | 156.884 | 171.472 | 193.504 |
| Dipole moment (μ) (Debye) | 6-31G (d) | 2.796 | 6.674 | 5.631 | 2.864 | 1.287 |
| | 6-31G (d, p) | 2.785 | 6.674 | 5.631 | 2.852 | 0.854 |
| Polarizability ($\alpha \times 10^{-39}$ in $C^3m^3J^{-1}$) | 6-31G (d) | 1.435 | 4.400 | 4.181 | 4.459 | 4.807 |
| | 6-31G (d, p) | 1.441 | 4.470 | 4.197 | 4.472 | 4.845 |

### 3.2. ESP analysis

In computer-aided drug design, the atomic charges are employed to investigate the connectivity between the structure and biological activity of the drug [60]. In the quantum mechanical illustration, the electrostatic properties of a molecule are represented through atom centered point charges. Mulliken, Hirshfeld, and NBO population analysis are usually used to calculate the atomic partial charges [61-63].

The calculated partial charge of atoms for PH 2 is illustrated in the graph represented in figure 4 (Table 8).

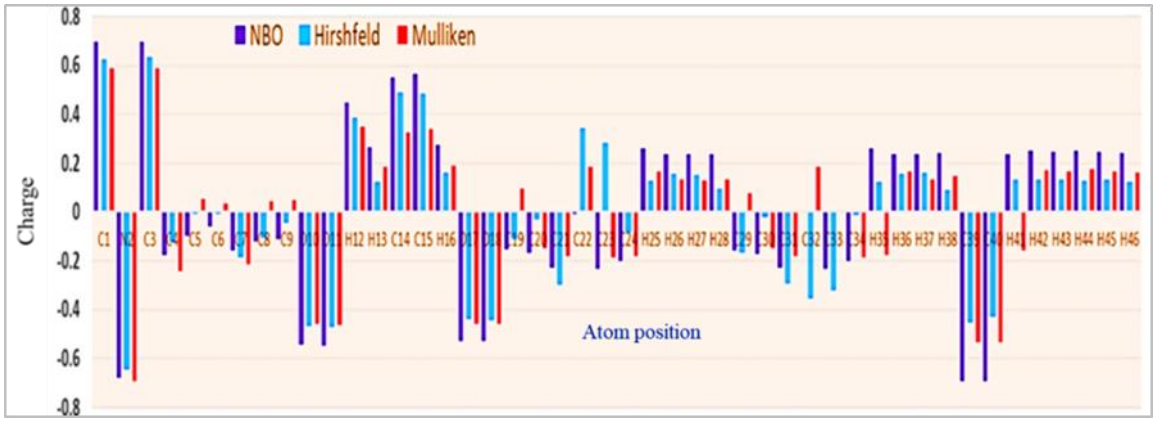


**Figure 4.** Graph of partial atomic charges of PH 2 computed with NBO, Hirshfeld, and Mulliken approaches

**Table 8.** Partial atomic charges of PH 2 computed with NBO, Hirshfeld and Mulliken approaches

| Atom | ESP | Mulliken | NBO | Atom | ESP | Mulliken | NBO |
|---|---|---|---|---|---|---|---|
| 1 C | 0.621 | 0.589 | 0.695 | 25 H | 0.122 | 0.166 | 0.259 |
| 2 N | -0.641 | -0.691 | -0.68 | 26 H | 0.151 | 0.132 | 0.238 |
| 3 C | 0.631 | 0.587 | -0.695 | 27 H | 0.147 | 0.128 | 0.236 |
| 4 C | -0.121 | -0.242 | -0.174 | 28 H | 0.090 | 0.134 | 0.237 |
| 5 C | -0.004 | 0.053 | -0.098 | 29 C | -0.160 | 0.077 | -0.158 |
| 6 C | 0.000 | 0.037 | -0.061 | 30 C | -0.018 | -0.149 | -0.17 |
| 7 C | -0.179 | -0.216 | -0.158 | 31 C | -0.290 | -0.181 | -0.23 |
| 8 C | -0.099 | 0.046 | -0.121 | 32 C | 0.351 | 0.186 | -0.002 |
| 9 C | -0.038 | 0.049 | -0.111 | 33 C | -0.317 | -0.187 | -0.233 |
| 10 O | -0.461 | -0.456 | -0.541 | 34 C | -0.005 | -0.177 | -0.199 |
| 11 O | -0.468 | -0.463 | -0.547 | 35 H | 0.119 | 0.167 | 0.259 |
| 12 H | 0.382 | 0.350 | 0.447 | 36 H | 0.150 | 0.135 | 0.239 |
| 13 H | 0.118 | 0.183 | 0.267 | 37 H | 0.156 | 0.134 | 0.239 |
| 14 C | 0.484 | 0.327 | 0.552 | 38 H | 0.085 | 0.146 | 0.242 |
| 15 C | 0.481 | 0.340 | 0.563 | 39 C | -0.450 | -0.532 | -0.691 |
| 16 H | 0.157 | 0.188 | 0.272 | 40 C | -0.424 | -0.533 | -0.693 |
| 17 O | -0.434 | -0.458 | -0.528 | 41 H | 0.119 | 0.159 | 0.232 |
| 18 O | -0.437 | -0.454 | -0.528 | 42 H | 0.130 | 0.172 | 0.249 |
| 19 C | -0.104 | 0.094 | -0.151 | 43 H | 0.127 | 0.166 | 0.245 |
| 20 C | -0.025 | -0.147 | -0.168 | 44 H | 0.125 | 0.175 | 0.251 |
| 21 C | -0.292 | -0.181 | -0.228 | 45 H | 0.119 | 0.167 | 0.246 |
| 22 C | 0.341 | 0.186 | -0.007 | 46 H | 0.118 | 0.162 | 0.241 |
| 23 C | -0.277 | -0.184 | -0.238 | | | | |
| 24 C | -0.079 | -0.182 | -0.2 | | | | |

Population analyses by NBO and Mulliken methods are connected with molecular orbital computation, whereas the Hirshfeld method is dependent on the electron density distribution. These methods innately suffer in a few inconsistencies. For example, Mulliken charge analyses are susceptible to the basis set. Employing this method for the evolution of atomic charges for the different levels of theories is not feasible. Moreover, the computed population can have a negative metaphysical number. One of the essential advantages of this method is that it requires less computation cost. Alternatively, NBO charges are inclined to be the largest in a degree, even though they demonstrate dynamic in electron population analysis against altering the basis set [64].

Hirshfeld partition scheme generates overlapping, non-spatially confined atomic fragments. However, it fails to predict consistent intermolecular and intramolecular charge trends in several systems [65]. It is evident from this work that in many contexts, carbon atoms reveal the most significant magnitude of charges in the NBO method. Most of the atoms demonstrate similarity in charge analysis by these three methods. Although the atom C22 in Hirshfeld and Mulliken analysis discloses a positive charge, a negative charge is observed in NBO analysis. Therefore, it can be claimed that electron population analysis employing various methods requires an emphasis on evaluating different systems.

In the ESP map, for a given chemical structure, the color intensity represents the ESP energy (in Hartrees) at a point on the electron density surface. In this type of illustration, red color indicates a maximum negative region, which is a promising site for an electrophilic attack, while the blue color signifies the maximum positive region favorable for

nucleophilic attack. It is evident from the calculated MEP map of ligand PH 2 (Figure 5) a maximum negative potential (-5.37 × $10^{-2}$ Hartree) region is over electronegative atom O10, and this region is likely to form hydrogen bonding with the amino acid residue of PAK 1 kinase. Later, the assumed interaction was detected in molecular docking simulation interactions analysis of PAK 1-PH 2 complexes through >N-H of the residue Leu347 and >C=O of phthalimide. On the contrary, the maximum positive potential (+5.37×$10^{-2}$ Hartree) region is located over electropositive atom H 12, which confirms the acceptor potency in forming hydrogen bonding with the amino acid residue Glu345 in PAK 1- PH 2 complex.

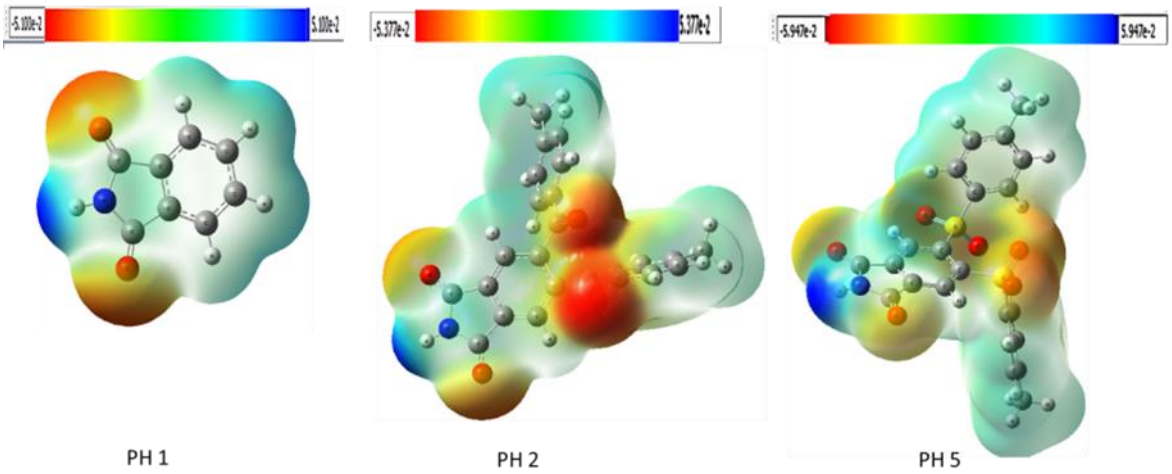


**Figure 5.** ESPs of PH 1, PH 2, and PH 5. The Blue region represents maximum positive potential, and the red region represents maximum negative potential

### 3.3. Frontier molecular orbitals and Chemical descriptor analysis

The computed $\varepsilon_{LUMO}$, $\varepsilon_{HOMO}$ and ΔE gap, Chemical Potential (μ), Electronegativity (χ), Hardness (η), Softness (S) and global Electrophilicity ($\omega$) were calculated for PH 1-5 (in eV) at B3LYP/6-31G (d) and B3LYP/6-31G (d, p) level theories (Table 9, 10 and Fig. 6). Gauss-Sum Program was manipulated to compute group contribution to the molecular orbitals (HOMO and LUMO) expressing in terms of the density of states (DOS) as displayed in Figure 7 [66]. The DOS plot presents a graphic analysis of the molecular orbital contribution, computed at B3LYP/6-31G (d) level theory. The positive sign of DOS indicates the LUMO, and the negative sign is for HOMO. Chemical susceptibility of a molecule is determined by the HOMO-LUMO energy gap, and the sizeable HOMO-LUMO gap signposts the high kinetic and chemical stability [67, 68]. This research calculates that the HOMO-LUMO gap in PH 1 is 5.038 eV. For the derivatives PH 2-5, this energy gap varies from 3.822 to 4.129 eV, representing all derivatives are more reactive than PH 1. The main reason for soaring the chemical reactivity is notified as that adding the substituent groups in 5 and 6 positions of phthalimide.

**Table 9**. εLUMO, εHOMO, and ΔE gap in eV are calculated for PH 1-5 at B3LYP/6-31G (d) and B3LYP/6-31G (d, p) level theory

| Entry | Basis set | Properties | | |
|---|---|---|---|---|
| | | εLUMO (eV) | εHOMO (eV) | ΔE gap (eV) |
| PH 1 | 6-31G (d) | -2.264 | -7.302 | 5.038 |
| | 6-31G (d, p) | -2.271 | -7.303 | 5.033 |
| PH 2 | 6-31G (d) | -2.717 | -6.751 | 3.822 |
| | 6-31G (d, p) | -2.715 | -6.753 | 4.037 |
| PH 3 | 6-31G (d) | -2.808 | -6.926 | 4.120 |
| | 6-31G (d, p) | -2.810 | -6.934 | 4.124 |
| PH 4 | 6-31G (d) | -3.020 | -7.068 | 4.033 |
| | 6-31G (d, p) | -3.018 | -7.073 | 4.055 |
| PH 5 | 6-31G (d) | -3.010 | -7.115 | 4.105 |
| | 6-31G (d, p) | -2.972 | -7.072 | 4.129 |

Frontier orbitals' energy value determines the drug's chemical reactivity and its tendency to bind with a given protein. In PH2, the electron-donating methyl groups are accumulated at the para positions of each phenyl ring decreases these orbital energy gaps to 3.822 eV. The reduced HOMO-LUMO energy gap contributes to forming PAK 1-PH2 complex yielding higher binding free energy.

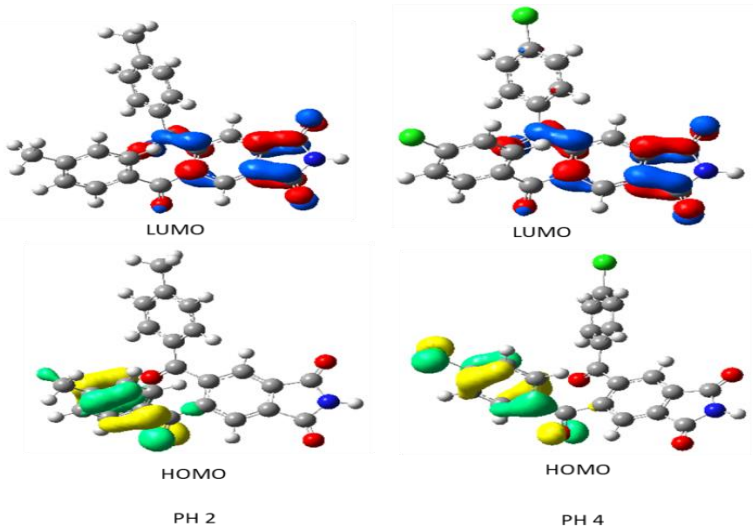


**Figure 6**. Frontier molecular orbitals (HOMO and LUMO) of PH 2 and PH 4 with isovalue = 0.05

It is evident from this calculation that PH2 displays the most significant softness (0.496 eV) and the least hardness (2.017 eV) among all reported systems (Table 10). The electrophilicity index also discloses the reactivity of the compound. On the other hand, PH1 shows the highest hardness among investigated compounds.

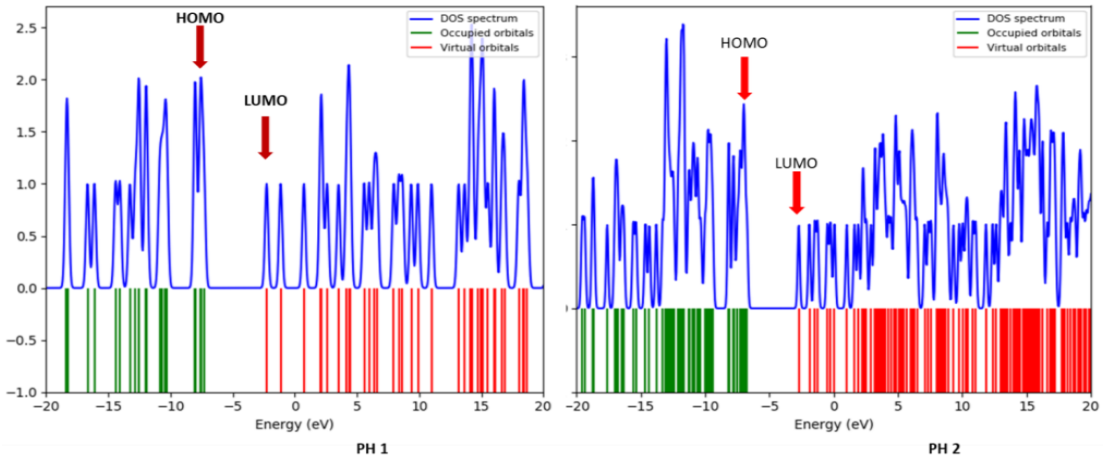


**Figure 7**. Computed total electron density of states diagram of PH 1 (left) and PH 2 (right)

**Table 10.** Chemical Potential (μ, eV), Electronegativity (χ, eV), Hardness (η , eV), Softness (S, eV$^{-1}$) and Electrophilicity ($\omega$, eV) for PH 1-5 calculated at B3LYP/6-31G (d) and B3LYP/6-31G (d, p) level theories

| Entry | Basis set | Properties | | | | |
|---|---|---|---|---|---|---|
| | | Chemical Potential (μ) | Electronegativity (χ) | Hardness (η ) | Softness (S) | Electrophilicity ($\omega$) |
| PH 1 | 6-31G (d) | -4.783 | 4.783 | 2.519 | 0.397 | 4.540 |
| | 6-31G (d, p) | -4.787 | 4.787 | 2.516 | 0.397 | 4.554 |
| PH 2 | 6-31G (d) | -4.734 | 4.734 | 2.017 | 0.496 | 5.556 |
| | 6-31G (d, p) | -4.734 | 4.734 | 2.019 | 0.495 | 5.551 |
| PH 3 | 6-31G (d) | -4.867 | 4.867 | 2.059 | 0.486 | 5.751 |
| | 6-31G (d, p) | -4.872 | 4.872 | 2.062 | 0.485 | 5.757 |
| PH 4 | 6-31G (d) | -5.044 | 5.044 | 2.024 | 0.494 | 6.284 |
| | 6-31G (d, p) | -5.046 | 5.046 | 2.027 | 0.493 | 6.279 |
| PH 5 | 6-31G (d) | -5.063 | 5.063 | 2.052 | 0.487 | 6.244 |
| | 6-31G (d, p) | -5.022 | 5.022 | 2.050 | 0.488 | 6.151 |

### 3.4. Fukui function analysis

The local chemical descriptor, like the Fukui function, directs the preferred position, where a chemical species will alter its density when the number of electrons is revised [45, 69]. Unlike substituents or functional groups, the condensed Fukui function and condensed local softness allow us to recognize each part of the molecule based on its divergent biochemical behavior. Parr and Yang confirmed the atoms in a given chemical system with the most significant values of the Fukui function ($f_k$) shows high reactivity for corresponding attacks. Accordingly, the site for nucleophilic attack will be the place where the value of $f^+$ is a maximum, while the value of f directs the site for an electrophilic attack(Table 11).

**Table 11**. Condensed Fukui Functions, local hardness, and local electrophilicity for PH 1-5 estimated in the atomic unit (a. u) at B3LYP/6-31G (d) level theory

| Entry | Atom | $f_k^+$ | $f_k^-$ | $f_k^0$ | $s_k^+$ | $s_k^-$ | $\omega_k^+$ | $\omega_k^-$ |
|---|---|---|---|---|---|---|---|---|
| | 2 N | 0.007 | 0.245 | 0.126 | 0.071 | 2.649 | 0.001 | 0.041 |
| | 5 C | 0.075 | 0.176 | 0.125 | 0.811 | 1.897 | 0.013 | 0.029 |
| PH 1 | 6 C | 0.075 | 0.176 | 0.125 | 0.811 | 1.897 | 0.013 | 0.029 |
| | 10 O | 0.141 | 0.110 | 0.125 | 1.522 | 1.186 | 0.024 | 0.018 |
| | 11 O | 0.141 | 0.110 | 0.125 | 1.522 | 1.186 | 0.024 | 0.018 |
| | 13 O | 0.095 | 0.050 | 0.073 | 1.357 | 0.717 | 0.022 | 0.012 |
| PH 2 | 26 O | 0.050 | 0.128 | 0.089 | 0.718 | 1.829 | 0.012 | 0.030 |
| | 27 C | 0.090 | 0.005 | 0.047 | 1.281 | 0.067 | 0.021 | 0.001 |
| | 13 O | 0.094 | 0.055 | 0.075 | 1.247 | 0.727 | 0.020 | 0.012 |
| PH 3 | 26 O | 0.047 | 0.162 | 0.104 | 0.620 | 2.133 | 0.010 | 0.034 |
| | 27 C | 0.101 | 0.019 | 0.060 | 1.333 | 0.245 | 0.021 | 0.004 |
| | 27 Cl | 0.058 | 0.138 | 0.098 | 0.776 | 1.865 | 0.013 | 0.032 |
| PH 4 | 28 C | 0.094 | -0.001 | 0.046 | 1.265 | -0.018 | 0.022 | 0.000 |
| | 40 Cl | 0.079 | 0.123 | 0.101 | 1.063 | 1.656 | 0.018 | 0.028 |
| | 11 S | 0.464 | -0.427 | 0.019 | 6.152 | -5.658 | 0.107 | -0.098 |
| PH 5 | 12 C | -0.135 | 0.255 | 0.060 | -1.789 | 3.382 | -0.031 | 0.059 |
| | 26 O | 0.108 | 0.042 | 0.075 | 1.436 | 0.557 | 0.025 | 0.010 |

For nucleophilic attack, the most reactive site is at O (10) and O (13) atoms in pyrrolidine ring in PH 1 and PH 2 respectively; C (27) and C (28) atoms of carbonyl group are connected with the phthalimide and aromatic ring in PH 3 and PH 4 respectively; and S (11) atom ($f_k^+$=0.4640) in -$SO_2$- group in compound PH 5. It was clear from this calculation, S (11) in PH 5 shows the most considerable softness ($s_k^+$= 6.1516; $\omega_k^+$= 0.1065) for nucleophilic attack than all other atoms in the present analysis.

### 3.5. Molecular docking analysis

The interaction energy for each ligand was estimated for all the likely binding sites of the receptor 4DAW, giving numerous values of binding energies for each system. Interaction and binding affinities of compounds 1-5 with PAK1 kinase are given in Table 12.

**Table 12**. The binding energy of Isoindoline1,3-dione and its derivatives against PAK1 protein.

| Entry | PH 1 | PH 2 | PH 3 | PH 4 | PH 5 |
|---|---|---|---|---|---|
| PAK1-Ligand binding energy (kcal/mol) | -5.5 | -7.3 | -7.4 | -7.4 | -7.7 |

Nevertheless, we have selected the values corresponding to the first posture as they overlay most appropriately with the experimental co-crystal structure of the phthalimide derivative-PAK1 complex [19, 52]. All five compounds are observed to dock in a cavity lined by Val284, Ala297, Arg299, Val328, Met344, Glu345, Tyr346, Leu347, Ser351, Asp393, Leu396, Thr406, and Asp407. This molecular docking analysis reveals that the ligand molecules PH 1-5 can form conventional and non-conventional hydrogen bonds, alkyl-π, σ-π, anion-π, and π-π interactions with PAK1(Table 13).

**Table 13**. A molecular docking simulation study of nonbonding interaction of PAK 1-phthalimide complexes

| | Conventional Hydrogen Bond | | Non-conventional Hydrogen Bond | | Hydrophobic | | Electrostatic | |
|---|---|---|---|---|---|---|---|---|
| **Entry** | **Amino acid-Ligand functional** | **Distance (Å)** | **Amino acid-Ligand functional** | **Distance (Å)** | **Amino acid-Ligand functional** | **Distance (Å)** | **Amino acid-Ligand functional** | **Distance (Å)** |
| PH 1 | Glu345(>C=O..H-N<) | 2.42 | Tyr346($H_2$CH..O=C<) | 2.37 | Val284(Sigma…PI) | 2.91 | | |
| | Leu347(>N-H..O=C<) | 1.91 | | | Ala297(Alkyl…Pi) | 3.36 & 4.40 | | |
| | | | | | Leu396(Alkyl …Pi) | 4.89 | | |
| PH 2 | Glu345(>C=O..H-N<) | 2.23 | Tyr346($H_2$CH..O=C<) | 2.72 | Val284(Alkyl …Pi) | 4.70 | Asp407(COO⁻..Pi) | 4.55 |
| | Arg299(>N-H..O=C<) | 2.92 | | | Ala297(Alkyl …Pi) | 3.95 & 4.95 | | |
| | Leu347(>N-H..O=C<) | 2.63 | | | Leu396(Alkyl …Pi) | 4.87 & 5.37 | | |
| | Thr406(-O-H…O=C<) | 2.60 | | | Val328(Alkyl …Pi ) | 5.21 | | |
| | | | | | Met344(Alkyl ..Pi ) | 5.20 | | |
| PH 3 | Asp393(>C=O..H-N<) | 2.69 | | | Arg299(Alkyl …Pi) | 5.35 | | |
| | Ser351(-O-H…O=C<) | 2.53 & 2.80 | | | Val284(Alkyl …Pi) | 5.17 | | |
| | | | | | Ala297(Alkyl …Pi) | 4.92 & 4.94 | | |
| | | | | | Leu396(Sigma..Pi) | 4.46 | | |
| | | | | | Met344(Alkyl ..Pi ) | 5.34 | | |
| PH 4 | Glu345(>C=O..H-N<) | 2.05 | Tyr346($H_2$CH..O=C<) | 3.63 | Val284(Alkyl …Pi) | 4.73 | Asp407(COO⁻.Pi) | 4.63 |
| | Arg299(>N-H..O=C<) | 2.96 | | | Ala297(Alkyl …Pi) | 3.84 & 4.80 | | |
| | Leu347(>N-H.O=C<) | 2.40 | | | Leu396(Alkyl …Pi) | 4.81 & 5.27 | | |
| | | | | | Val328(Alkyl …Pi) | 5.19 | | |
| | | | | | Met344(Alkyl …Pi) | 5.30 | | |
| PH 5 | Glu345(>C=O..H-N<) | 2.85 | | | Val284(Alkyl …Pi) | 4.85 | Asp407(COO⁻..Pi) | 4.11 |
| | Arg299(>N-H..O=C<) | 2.78 | | | Ala297(Alkyl …Pi) | 4.88 | | |
| | Thr406(-O-H…O=C<) | 1.98 | | | Val328(Alkyl …Pi) | 5.28 | | |
| | | | | | Met344(Alkyl …Pi) | 4.96 | | |
| | | | | | Leu396(Sigma..Pi) | 5.01 | | |

The binding energy of PH 1 is -5.5 kcal/mol, whereas introducing two aryl groups to the parent scaffold PH 1 significantly increases the strength of hydrogen bonding and other nonbonding interactions with the PAK1.

As a consequence, the binding affinities with PAK1 significantly increase to -7.3, -

7.4, -7.4, and -7.7 kcal/mol for PH 2-5, respectively.

Hydrogen-bonds execute a vital function in shaping the specificity of ligand binding with the receptor, drug design in chemical and biological processes, molecular recognition, and biological activity [70]. The molecular docking analysis revealed that isoindoline forms two conventional hydrogen bonds with amino acid residues Glu345, Leu347 and one non-conventional hydrogen bond (A contact A—H···B wherein a H atom develops a non-covalent bond in the middle of two structural moieties A and B, of which one or even both are only of moderate to low electronegativity) with Tyr346 of PAK1 receptor. The highest binding affinities (-7.7 kcal/mol) is estimated for PH 5, which fabricates hydrogen bonding with Glu345, Arg299, and Thr406.

A recent study revealed that hydrogen bonds of less than 2.3 Å could amplify binding affinities by several orders of magnitude [71]. Therefore, the hydrogen bond detected between Thr406 and PH 5 with the functionals $H_2C$-H and O=C= (1.98 Å) might play a crucial role in ligand-receptor binding potency. However, the non-covalent contact concerning an electron-deficient aromatic ring and an anion appropriately placed above the ring plane is termed anion-π interaction [72]. This type of interaction is electrostatic and can play a crucial role in a biological system such as inhibition of the enzymatic activity of urate oxidase [73]. In this docking analysis, some protein residues such as Asp and Glu are involved in a considerable number of anion- π interactions with a selected close-to-parallel alignment of their carboxylate group concerning interacting aromatic system [74]. This study revealed that an interaction exists between a carboxylate ion of Asp407 and π electrons of the phenyl group of the PH 2 and PH 5 with bond distances of 4.55 and 4.11 Å, respectively. It may be inferred that the phenyl groups attached with isoindoline derivatives are electron-deficient and are involved in charge transfer from Asp407 to ligand, ensuing the inhibition of PAK1 kinase performance. It was evident from this investigation that PH 2-5 are involved in alkyl- π orbital or σ- π orbital type non-hydrophobic interactions with Val284, Ala297, Leu396 and some other amino acid residues of PAK1. Moreover, a π - π contacts between two phenyl groups is predicted for ligand PH 2, PH 4, and PH 5 in the PAK1-ligand complex with distances ranging from 3.62 to 3.66 Å (Figure 8, 9 and 10). This sort of interaction often facilitates stabilizing the three-dimensional structure of the complex [75].

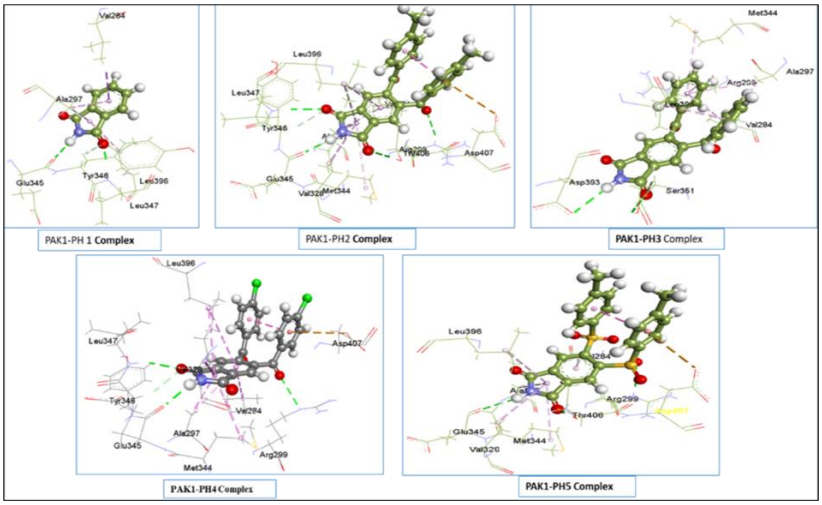


**Figure 8**. 3D representation of nonbonding interaction of PH 1 - 5 with 4DAW generated by Discovery Studio

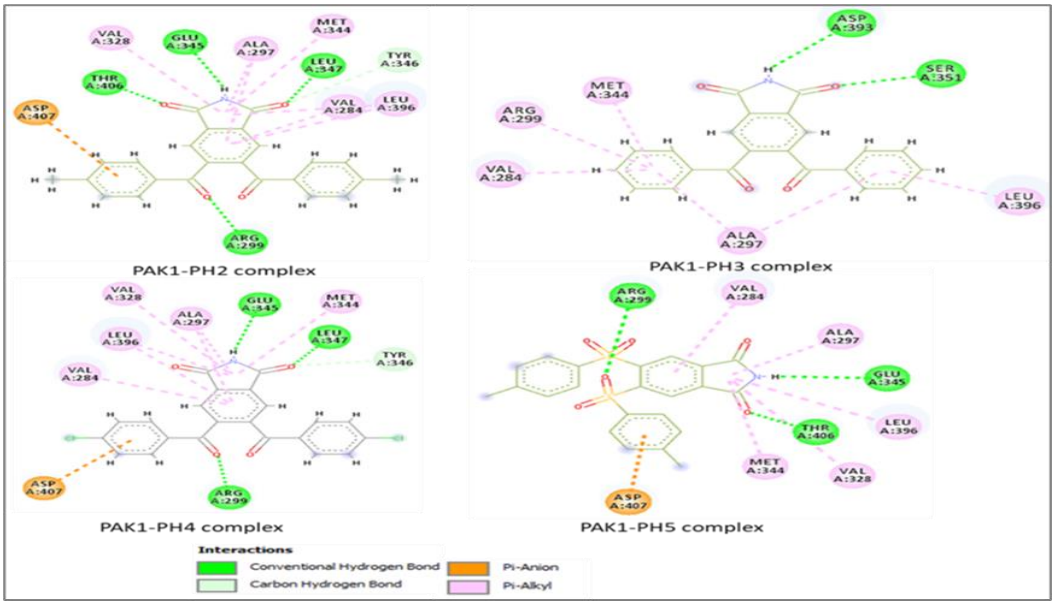


**Figure 9**. 2D representation of nonbonding interaction of PH 2, PH 3, PH 4, and PH 5 with amino acid residues of 4DAW generated by Discovery Studio

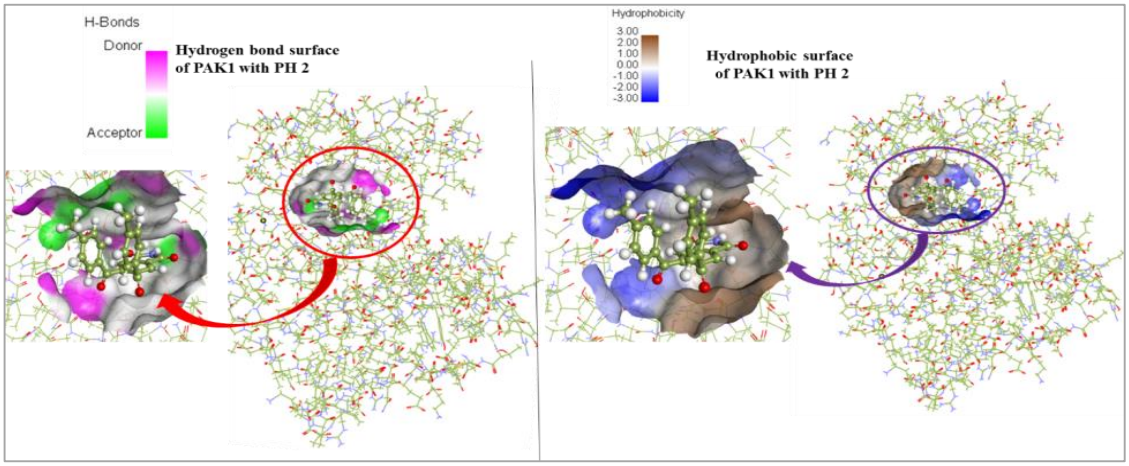


**Figure 10.** Hydrogen bond surface hydrophobic surface of PAK1 with PH 2

The superimposed outlook of all ligands (PH 2 - PH 5) after docking has been given in Figure 11. It reflects from this figure that all ligands are docked nearly the same location in protein pocket.

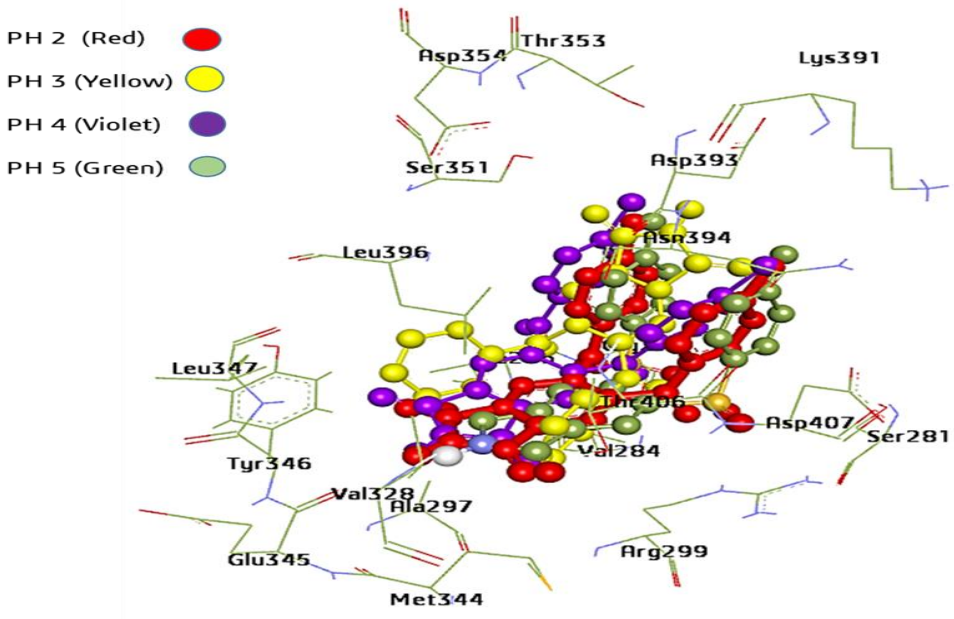


**Figure 11.** The superimposed complexes of PH 2 - PH 5 with PAK1

### 3.6. Pharmacokinetic properties

The five phthalimide derivatives were evaluated with the SwissADME and admetASR web tool to predict drug-likeness and pharmacokinetics properties, which are crucial for rational drug design. Generally, drug-likeness is evaluated using the Lipinski's rule of five [76]. As a matter of principle, an orally active drug should have no more than one interruption of the following conditions: (1) no more than five hydrogen bond donors, (2) no more than ten hydrogen bond acceptor, (3) molecular mass of less than 500 Da; and (4) an octanol-water partition coefficient of not more than five. As all the numbers of these recommendations are multiple of 5, the rules are termed Lipinski's rule of five. If two or more of the guidelines are disrupted, reduced absorption can be estimated. All phthalimide ligands do not violate Lipinski's rule and data has been presented in Table 14.

**Table 14.** Predicted oral bioavailable parameter of PH 1-5

| Entry | MW (g/mol) | Log $P_{o/w}$ (XLOGP3) | NHA | NHD | NRB | TPSA (Å²) | Csp3 |
|---|---|---|---|---|---|---|---|
| PH 1 | 147.13 | 1.15 | 2 | 1 | 0 | 46.17 | 0 |
| PH 2 | 383.40 | 4.13 | 4 | 1 | 4 | 80.31 | 0.08 |
| PH 3 | 355.34 | 3.40 | 4 | 1 | 4 | 80.31 | 0 |
| PH 4 | 424.23 | 4.66 | 4 | 1 | 4 | 80.31 | 0 |
| PH 5 | 487.50 | 3.64 | 8 | 1 | 6 | 149.67 | 0.09 |
| Reference ligand | 150 to 500 | -0.7 to +5.0 | ≤ 10 | ≤ 5 | ≤ 9 | 20 to 130 | ≥ 0.25 |

Note: MW, molecular weight; NHD, No. of H-bond donors; NHA, No. of H-bond acceptor; NRB, no. of rotatable bonds; TPSA, topological polar surface area; Csp3, the fraction of sp3 carbon atom.

Lipophilicity determines how easily the drug passes through the lipid membrane. It is estimated from the partition-coefficient of a drug in octanol and water medium (Log Po/w). For an excellent bioavailability of a drug-like

molecule, lipophilicity value generally varies between −0.7 and +5.0. It is clear from this study that all investigated compounds possess an excellent lipophilicity index from 1.15 to 4.66. Similarly, NHD and NHA determine the maximum number of hydrogen bond-forming ability, and NRB controls the flexibility of the drug molecule. The estimated values for ligands PH 1 to PH 5 show good agreement with their optimal range for NHD, NHA, and NRB. However, the fraction of sp3 carbon atoms that governs the fraction of saturation in a molecule shows much smaller values than optimal magnitude (≥ 0.25). However, topological polar surface area (TPSA) is likewise employed as a contributing factor for oral absorption, and blood-brain barrier permeation capacity and the screened drug-likeness of a molecule should have TPSA between 20 and 130 $Å^2$. The SwissADME web tool predication ravels that only the ligand PH 5 violates this standard, and the leftover four phthalimide derivatives are anticipated to be orally bioavailable.

The variation of molecular and physicochemical properties, such as molecular weight (MW), lipophilicity (Log Po/w), Number of rotational bond (NRB), topological polar surface area (PSA) and saturation (Csp3) of the compounds PH 1 to PH 5 can be represented by bioavailability radar diagram (Figure 12). It is clear from the graph that PH 5 has the highest molecular weight with the highest NRB. On the other hand, PH 2-4 has the same NRB though they possess various molecular weights. In case of lipophilicity, the preference PH 4 > PH 2 >PH 5 > PH 3 is predicated. Nearly a similar trend is found for TPSA and Csp3. This study predicts that molecular structural features govern the bioavailability of a given molecule.

As determined by AdmetSAR prediction [58], the four ligands PH 1, PH 2, PH 3, and PH 4 are perceived to be noncancerous and have good passive gastrointestinal absorption. Some selected pharmacokinetic parameter has been reported in Table 15.

**Table 15.** Selected pharmacokinetic parameter of PH 1-5

| Entry | BBB | HIA | Caco-2 (cm/s) | PGI | CYP450 2D6 | hERG | Carcinogen | AM | FAT |
|---|---|---|---|---|---|---|---|---|---|
| PH 1 | +ve (0.998) | +ve (1.00) | +ve (1.663) | NI (0.973) | NS (0.804) | WI (0.984) | NC (0.948) | -ve (0.9100) | -ve (0.7348) |
| PH 2 | +ve (0.986) | +ve (1.00) | +ve (1.478) | NI (0.936) | NS (0.834) | WI (0.985) | NC (0.911) | -ve (0.7200) | +ve (0.8142) |
| PH 3 | +ve (0.994) | +ve (1.00) | +ve (1.373) | NI (0.947) | NS (0.827) | WI (0.982) | NC (0.933) | -ve (0.8000) | + ve (0.7672) |
| PH 4 | +ve (0.993) | +ve (1.00) | +ve (1.415) | NI (0.963) | NS (0.848) | WI (0.976) | NC (0.833) | -ve (0.7600) | +ve (0.9205) |
| PH 5 | +ve (0.946) | +ve (1.00) | -ve (0.864) | NI (0.841) | NS (0.848) | WI (0.807) | C (0.713) | -ve (0.8200) | +ve (0.9815) |

Note: BBB, blood-brain barrier; HIA, human intestinal absorption; Caco-2, Cyprotex's Caco-2 permeability; PGI, P-glycoprotein Inhibitor; hERG, human ether-a-go-go-related gene inhibition; NC, non-carcinogens; C, carcinogens; +ve, permeable; NS, Non-substrate; NI, non-inhibitor; WI, weak inhibitor; AM, Ames mutagenesis; FAT, fish aquatic toxicity.

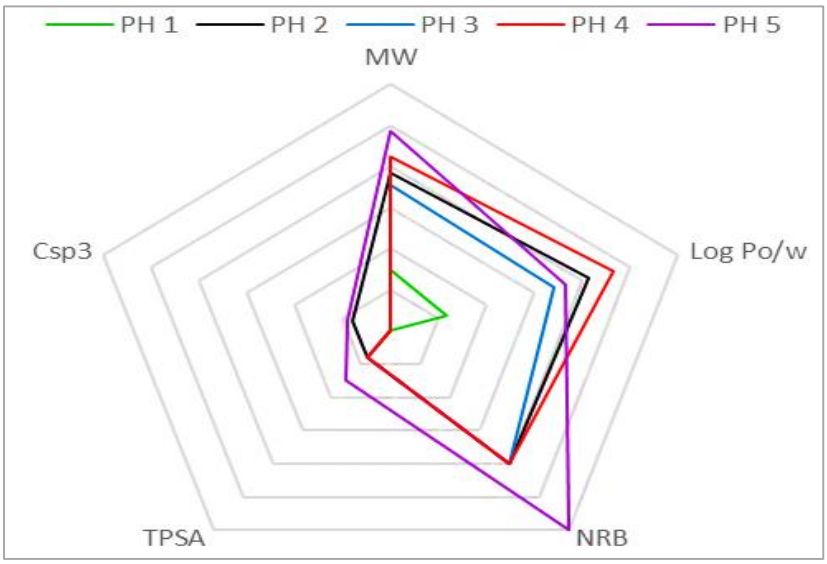


**Figure 12.** The diagram represents the relation between molecular weight, no. of rotatable bonds, Log $P_{o/w,}$ topological polar surface area and the fraction of sp3 carbon atom

However, compound PH 5 was found to be carcinogenic. Moreover, all the ligand molecules showed a negative ames mutagenesis as predicted by this calculation, indicating these compounds will not cause mutation in DNA. The perception about compounds being substrate or non-substrate of the permeability glycoprotein is a major factor in evaluating active efflux through the biological membrane, such as from gastrointestinal wall to the lume [77, 78]. As predicted by AdmetSAR, all screened compounds in this work were found to be non-inhibitor P-glycoprotein inhibitors. However, all the selected compounds show weak inhibition of human ether-a-go-go-related gene and good blood-brain barrier permeation. However, fish aquatic toxicity prediction shows that these compounds may harm aquatic ecology.

However, compound PH 5 was found to be carcinogenic. Moreover, all the ligand molecules showed a negative ames mutagenesis as predicted by this calculation, indicating these compounds will not cause mutation in DNA. The perception about compounds being substrate or non-substrate of the permeability glycoprotein is a significant factor in evaluating active efflux through biological membranes, such as from gastrointestinal wall to the lumen. As predicted by AdmetSAR, all screened compounds in this work were found to be non-inhibitor P-glycoprotein inhibitors. However, all the selected compounds show weak inhibition of human ether-a-go-go-related gene and good blood-brain barrier permeation. However, fish aquatic toxicity prediction shows that these compounds may harm aquatic ecology.

## 4. Conclusions

In this research, DFT analysis, molecular docking, and ADMET predictions are employed to evaluate 5, 6-diaroylisoindoline-1, 3-dione as PAK1 kinase inhibitors, and anti-carcinogenic potential therapeutics. Among the investigated phthalimide derivatives, non-covalent interactions, such as hydrogen bonding, hydrophobic, electrostatic, anion-π, and π-π interactions for PH 2-4, were nearly similar. The highest binding scores using Auto Dock Vina was found to be -7.7 (kcal/mol) for PH 5. Besides docking analysis, the DFT study predicts that all Gibbs free energy of all derivatives is

negative, and the HOMO-LUMO energy gap indicates that PH 2 is the most reactive ligand. The molecular electrostatic potential analysis also disclosed the most negative and positive surface area of the investigated molecule and hence, anticipated the probable site for the hydrogen bonding site. However, ADMET predictions suggest that PH 2-4 are orally bioavailable and non-carcinogenic.

## Abbreviations

Molecular weight (MW), lipophilicity (Log Po/w), Number of rotational bond (NRB), topological polar surface area (PSA), molecular docking study (MDS), Density functional theory (DFT) Highest Occupied Molecular Orbital (HOMO) and Lowest unoccupied Molecular Orbital (LUMO). PH1 (Isoindoline-1, 3-Dione); PH2 (5, 6-bis (4-methylbenzoyl) isoindoline-1, 3-Dione); PH3 (5, 6-dibenzoylisoindoline-1, 3-Dione); PH4 (5, 6-bis (4-chlorobenzoyl) isoindoline-1, 3-Dione); PH5 (di-p-tolyl 1, 3-dioxoisoindoline-5, 6-disulfonate).

## Conflict of interest

The authors declare no conflict of interest.

## Consent for publications

All authors read and approved the final manuscript for publication.

## Availability of data and material

The authors declare that they have embedded all data in the manuscript.

## Ethics approval and consent to participate

No human or animals were used in the present research.

## Author contributions

Hoque, M M, and Khan, M W organized the concept of this study. Hoque, M M executed quantum chemical computations, performed docking analysis, ADMET prediction analysis, executed data collection and analysis, and wrote the manuscript. Khan, M W supervised this work and reviewed the manuscript. Kumar, A, helped to analyze the DOS spectrum and data, and improved the manuscript. Hossain, M S, also revised the manuscript. All authors read and approved the manuscript.

## Acknowledgments

The authors thankfully confess for the funding of Bangladesh University of Engineering and Technology, Dhaka. The authors are also grateful to Dr. Mohammad A. Halim, Division of Computer-Aided Drug Design, The Red-Green Research Centre, BICCB, Dhaka, Bangladesh, to support his computational resources.

## References

1. Sells M A, Knaus U G, Bagrodia S, Ambrose D M, Bokoch G M, Chernoff J. (1997). Human p21-activated kinase (Pak1) regulates actin organization in mammalian cells. *Current Biology*, 7(3): 202-210.
2. Delorme V, Machacek M, DerMardirossian C, Anderson K L, Wittmann T, Hanein D, Waterman-Storer C, Danuser G, Bokoch G M. (2007). Cofilin activity downstream of Pak1 regulates cell protrusion efficiency by organizing lamellipodium and lamella actin networks. *Developmental cell*, 13(5): 646-662.
3. Adam L, Vadlamudi R, Kondapaka S B, Chernoff J, Mendelsohn J, Kumar R. (1998). Heregulin regulates cytoskeletal reorganization and cell migration through the p21-activated kinase-1 via phosphatidylinositol-3 kinase. *Journal of Biological Chemistry*, 273(43): 28238-28246.
4. Manser E, Leung T, Salihuddin H, Zhao Z-s, Lim L. (1994). A brain serine/threonine

protein kinase activated by Cdc42 and Rac1. *Nature*, 367(6458): 40-46.

5. Ma Q-L, Yang F, Frautschy S A, Cole G M. (2012). PAK in Alzheimer disease, Huntington disease and X-linked mental retardation. *Cellular logistics*, 2(2): 117-125.
6. Mendoza-Naranjo A, Gonzalez-Billault C, Maccioni R B. (2007). Aβ1-42 stimulates actin polymerization in hippocampal neurons through Rac1 and Cdc42 Rho GTPases. *Journal of cell science*, 120(2): 279-288.
7. Arber S, Barbayannis F A, Hanser H, Schneider C, Stanyon C A, Bernard O, Caroni P. (1998). Regulation of actin dynamics through phosphorylation of cofilin by LIM-kinase. *Nature*, 393(6687): 805-809.
8. Yang N, Higuchi O, Ohashi K, Nagata K, Wada A, Kangawa K, Nishida E, Mizuno K. (1998). Cofilin phosphorylation by LIM-kinase 1 and its role in Rac-mediated actin reorganization. *Nature*, 393(6687): 809-812. https://doi.org/10.1038/31735
9. Heredia L, Helguera P, de Olmos S, Kedikian G, Vigo F S, LaFerla F, Staufenbiel M, de Olmos J, Busciglio J, Cáceres A. (2006). Phosphorylation of actin-depolymerizing factor/cofilin by LIM-kinase mediates amyloid β-induced degeneration: a potential mechanism of neuronal dystrophy in Alzheimer's disease. *Journal of Neuroscience*, 26(24): 6533-6542.
10. Madzelan P, Labunska T, Wilson M A. (2012). Influence of peptide dipoles and hydrogen bonds on reactive cysteine pK a values in fission yeast DJ-1. *The FEBS journal*, 279(22): 4111-4120.
11. Balasenthil S, Sahin A A, Barnes C J, Wang R-A, Pestell R G, Vadlamudi R K, Kumar R. (2004). p21-activated kinase-1 signaling mediates cyclin D1 expression in mammary epithelial and cancer cells. *Journal of Biological Chemistry*, 279(2): 1422-1428.
12. Jagadeeshan S, Krishnamoorthy Y, Singhal M, Subramanian A, Mavuluri J, Lakshmi A, Roshini A, Baskar G, Ravi M, Joseph L. (2015). Transcriptional regulation of fibronectin by p21-activated kinase-1 modulates pancreatic tumorigenesis. *Oncogene*, 34(4): 455-464.
13. Kumar R, Gururaj A E, Barnes C J. (2006). p21-activated kinases in cancer. *Nature Reviews Cancer*, 6(6): 459-471.
14. Radu M, Semenova G, Kosoff R, Chernoff J. (2014). PAK signalling during the development and progression of cancer. *Nature Reviews Cancer*, 14(1): 13-25.
15. Takahashi H, Nguyen B C Q, Uto Y, Shahinozzaman M, Tawata S, Maruta H. (2017). 1, 2, 3-Triazolyl esterization of PAK1-blocking propolis ingredients, artepillin C (ARC) and caffeic acid (CA), for boosting their anti-cancer/anti-PAK1 activities along with cell-permeability. *Drug Discoveries & Therapeutics*.
16. Zhou Y, Zhang J, Wang J, Cheng M S, Zhao D M, Li F. (2019). Targeting PAK1 with the Small Molecule Drug AK963/40708899 Suppresses Gastric Cancer Cell Proliferation and Invasion by Downregulation of PAK1 Activity and PAK1-Related Signaling Pathways. *The Anatomical Record*, 302(9): 1571-1579.
17. Vamecq J, Bac P, Herrenknecht C, Maurois P, Delcourt P, Stables J P. (2000). Synthesis and anticonvulsant and neurotoxic properties of substituted N-phenyl derivatives of the phthalimide pharmacophore. *Journal of medicinal chemistry*, 43(7): 1311-1319.
18. Blanck S, Geisselbrecht Y, Kräling K, Middel S, Mietke T, Harms K, Essen L-O, Meggers E. (2012). Bioactive cyclometalated phthalimides: design, synthesis and kinase inhibition. *Dalton Transactions*, 41(31): 9337-9348.
19. Maksimoska J, Feng L, Harms K, Yi C, Kissil J, Marmorstein R, Meggers E. (2008). Targeting large kinase active site with rigid, bulky octahedral ruthenium complexes. *Journal of the American Chemical Society*, 130(47): 15764-15765.
20. Wang Y, Huang H, Zhang Q, Zhang P. (2018). Chirality in metal-based anticancer agents. *Dalton Transactions*, 47(12): 4017-4026.
21. Bollati M, Alvarez K, Assenberg R, Baronti C, Canard B, Cook S, Coutard B, Decroly E, de Lamballerie X, Gould E A. (2010). Structure and functionality in flavivirus NS-proteins: perspectives for drug design. *Antiviral research*, 87(2): 125-148.

22. Cheong P H-Y, Legault C Y, Um J M, Çelebi-Ölçüm N, Houk K. (2011). Quantum mechanical investigations of organocatalysis: mechanisms, reactivities, and selectivities. *Chemical reviews*, 111(8): 5042-5137.
23. Houk K N, Cheong P H-Y. (2008). Computational prediction of small-molecule catalysts. *Nature*, 455(7211): 309-313.
24. Niu S, Huang D-L, Dau P D, Liu H-T, Wang L-S, Ichiye T. (2014). Assessment of quantum mechanical methods for copper and iron complexes by photoelectron spectroscopy. *Journal of chemical theory and computation*, 10(3): 1283-1291.
25. Meng X-Y, Zhang H-X, Mezei M, Cui M. (2011). Molecular docking: a powerful approach for structure-based drug discovery. *Current computer-aided drug design*, 7(2): 146-157.
26. Hoque M M, Halim M A, Rahman M M, Hossain M I, Khan M W. (2013). Synthesis and structural insights of substituted 2-iodoacetanilides and 2-iodoanilines. *Journal of Molecular Structure*, 1054: 367-374.
27. Hoque M M, Halim M A, Sarwar M G, Khan M W. (2015). Palladium-catalyzed cyclization of 2-alkynyl-N-ethanoyl anilines to indoles: synthesis, structural, spectroscopic, and mechanistic study. *Journal of Physical Organic Chemistry*, 28(12): 732-742.
28. Pang X, Zhou L, Zhang L, Xu L, Zhang X. (2008). Two rules on the protein-ligand interaction. *Nature Precedings*: 1-1.
29. Parr R G, Yang W. (1984). Density functional approach to the frontier-electron theory of chemical reactivity. *Journal of the American Chemical Society*, 106(14): 4049-4050.
30. Politzer P, Truhlar D G. (2013). Chemical applications of atomic and molecular electrostatic potentials: reactivity, structure, scattering, and energetics of organic, inorganic, and biological systems: *Springer Science & Business Media*.
31. H. Weinstein, S. Maayani, S. Srebrenik, S. Cohen, Sokolovsky M. (1975). A theoretical and experimental study of the semirigid cholinergic agonist 3-acetoxyquinuclidine. *Molecular pharmacology*, 11(5): 671-689.
32. Lien E J, Guo Z, Ru, Li R, Li, Su C, Tang. (1982). Use of dipole moment as a parameter in drug-receptor interaction and quantitative structure and activity relationship studies. *Journal of pharmaceutical sciences*, 71(6): 641-655.
33. Romanelli G, Cafferata L, Castro E. (2000). An improved QSAR study of toxicity of saturated alcohols. *Journal of Molecular Structure: THEOCHEM*, 504(1-3): 261-265.
34. Hemdan M M, El S, Amira A. (2016). Synthesis of Some New Heterocycles Derived from Novel 2(1, 3 Dioxisoindolin 2 yl) Benzoyl Isothiocyanate. *Journal of Heterocyclic Chemistry*, 53(2): 487-492.
35. Deb M, Hazra S, Gupta A, Elias A J. (2018). Synthesis of unsymmetrical multi-aroyl derivatives of ferrocene using palladium catalysed oxidative C–H aroylation. *Dalton Transactions*, 47(21): 7229-7236.
36. Pünner F, Schieven J, Hilt G. (2013). Synthesis of fluorenone and anthraquinone derivatives from aryl-and aroyl-substituted propiolates. *Organic Letters*, 15(18): 4888-4891.
37. Nie Z, Ding Q, Peng Y. (2016). Synthesis of 6-aroyl phenanthridines by Fe-catalyzed oxidative radical cyclization of 2-isocyanobiphenyls with benzylic alcohols. Tetrahedron, 72(50): 8350-8357.
38. Parr R G, Pearson R G. (1983). Absolute hardness: companion parameter to absolute electronegativity. *Journal of the American Chemical Society*, 105(26): 7512-7516.
39. Frisch M, Trucks G, Schlegel H B, Scuseria G E, Robb M A, Cheeseman J R, Scalmani G, Barone V, Mennucci B, Petersson G. (2009). gaussian 09, Revision d. 01, Gaussian. Inc., Wallingford CT, 201.
40. Becke A D. (1992). Density functional thermochemistry. I. The effect of the exchange only gradient correction. *The Journal of chemical physics*, 96(3): 2155-2160.
41. Mulliken R S. (1935). Electronic structures of molecules XI. Electroaffinity, molecular orbitals and dipole moments. *The Journal of chemical physics*, 3(9): 573-585.
42. Pearson R G. (1986). Absolute electronegativity and hardness correlated with molecular orbital theory. *Proceedings of the National Academy of Sciences*, 83(22): 8440-8441.

43. Abu Saleh M, Solayman M, Hoque M M, Khan M A, Sarwar M G, Halim M A. (2016). Inhibition of DNA topoisomerase type IIα (TOP2A) by mitoxantrone and its halogenated derivatives: a combined density functional and molecular docking study. *BioMed research international*, 2016.
44. Koopmans T. (1934). Über die Zuordnung von Wellenfunktionen und Eigenwerten zu den einzelnen Elektronen eines Atoms. *physica*, 1(1-6): 104-113.
45. Parr R G, László v. Szentpály, Shubin Liu. (1999.). "Electrophilicity Index." *Journal of the American Chemical Society*, 21(9): 1922–1924.
46. Dykstra C E. (2000). Finding the way through intermolecular forces. Perspective on "Permanent and induced molecular moments and long-range intermolecular forces" Theoretical Chemistry Accounts (pp. 278-280): *Springer*.
47. Abraham J P, Sajan D, Joe I H, Jayakumar V. (2008). Molecular structure, spectroscopic studies and first-order molecular hyperpolarizabilities of p-amino acetanilide. *Spectrochimica Acta Part A: Molecular and Biomolecular Spectroscopy*, 71(2): 355-367.
48. Karamanis P, Pouchan C, Maroulis G. (2008). Structure, stability, dipole polarizability and differential polarizability in small gallium arsenide clusters from all-electron ab initio and density-functional-theory calculations. *Physical Review A*, 77(1): 013201.
49. Parr R G. (1980). Density functional theory of atoms and molecules Horizons of Quantum Chemistry (pp. 5-15): *Springer*.
50. Ayers P W, Parr R G. (2000). Variational principles for describing chemical reactions: the Fukui function and chemical hardness revisited. *Journal of the American Chemical Society*, 122(9): 2010-2018.
51. Yang W, Mortier W J. (1986). The use of global and local molecular parameters for the analysis of the gas-phase basicity of amines. *Journal of the American Chemical Society*, 108(19): 5708-5711.
52. Blanck S, Maksimoska J, Baumeister J, Harms K, Marmorstein R, Meggers E. (2012). The art of filling protein pockets efficiently with octahedral metal complexes. *Angewandte Chemie International Edition*, 51(21): 5244-5246.
53. DeLano W L. (2002). The PyMOL user's manual.
54. Guex N, Peitsch M C. (1997). SWISS-MODEL and the Swiss-Pdb Viewer: an environment for comparative protein modeling. *electrophoresis*, 18(15): 2714-2723.
55. Dundas J, Ouyang Z, Tseng J, Binkowski A, Turpaz Y, Liang J. (2006). CASTp: computed atlas of surface topography of proteins with structural and topographical mapping of functionally annotated residues. *Nucleic acids research*, 34(suppl_2): W116-W118.
56. Trott O O, Arthur J. (2010). AutoDock Vina: improving the speed and accuracy of docking with a new scoring function, efficient optimization, and multithreading. *Journal of Computational Chemistry*, 31(2): 455-461.
57. Inc A S. (2013). Discovery Studio Modeling Environment, release 4.0.
58. Cheng F, Li W, Zhou Y, Shen J, Wu Z, Liu G, Lee P W, Tang Y. (2012). admetSAR: a comprehensive source and free tool for assessment of chemical ADMET properties: ACS Publications.
59. Daina A, Michielin O, Zoete V. (2017). SwissADME: a free web tool to evaluate pharmacokinetics, drug-likeness and medicinal chemistry friendliness of small molecules. *Scientific reports*, 7: 42717.
60. Wilson L Y, Famini G R. (1991). Using theoretical descriptors in quantitative structure-activity relationships: some toxicological indices. *Journal of medicinal chemistry*, 34(5): 1668-1674.
61. Mulliken R S. (1955). Electronic population analysis on LCAO–MO molecular wave functions. I. *The Journal of chemical physics*, 23(10): 1833-1840.
62. Demircioğlu Z, Kaştaş Ç A, Büyükgüngör O. (2015). Theoretical analysis (NBO, NPA, Mulliken Population Method) and molecular orbital studies (hardness, chemical potential, electrophilicity and Fukui function analysis) of (E)-2-((4-hydroxy-2-methylphenylimino) methyl)-3-methoxyphenol. *Journal of Molecular Structure*, 1091: 183-195.
63. Shawon J, Khan A M, Rahman A, Hoque M M, Khan M A K, Sarwar M G, Halim M A.

(2018). Molecular recognition of azelaic acid and related molecules with DNA polymerase I investigated by molecular modeling calculations. *Interdisciplinary Sciences: Computational Life Sciences*, 10(3): 525-537.

64. Rodríguez-Spong B, Price C P, Jayasankar A, Matzger A J, Rodríguez-Hornedo N r. (2004). General principles of pharmaceutical solid polymorphism: a supramolecular perspective. *Advanced drug delivery reviews*, 56(3): 241-274.
65. Saha S, Roy R K, Ayers P W. (2009). Are the Hirshfeld and Mulliken population analysis schemes consistent with chemical intuition? *International journal of quantum chemistry*, 109(9): 1790-1806.
66. Tenderholt A, Langner K, O'Boyle N. (2008). A library for package-independent computational chemistry algorithms. *J. Comp. Chem*: 839-845.
67. Rahman A, Hoque M M, Khan M A, Sarwar M G, Halim M A. (2016). Non-covalent interactions involving halogenated derivatives of capecitabine and thymidylate synthase: a computational approach. *SpringerPlus*, 5(1): 146.
68. Uddin N, Ahmed S, Khan A M, Mazharol Hoque M, Halim M A. (2020). Halogenated derivatives of methotrexate as human dihydrofolate reductase inhibitors in cancer chemotherapy. *Journal of Biomolecular Structure and Dynamics*, 38(3): 901-917.
69. Parr R G C, Pratim K;. (1991). Principle of maximum hardness. *Journal of the American Chemical Society*, 113(5): 1854-1855.
70. Perlstein J. (2001). The Weak Hydrogen Bond In Structural Chemistry and Biology (International Union of Crystallography, Monographs on Crystallography, 9) By Gautam R. Desiraju (University of Hyderabad) and Thomas Steiner (Freie Universität Berlin). Oxford University Press: Oxford and New York. 1999. xiv+ 507 pp. $150. ISBN 0-19-850252-4: ACS Publications.
71. Wade R C, Goodford P J. (1989). The role of hydrogen-bonds in drug binding. *Progress in clinical and biological research*, 289: 433-444.
72. Quiñonero D, Garau C, Rotger C, Frontera A, Ballester P, Costa A, Deyà P M. (2002). Anion–π interactions: do they exist? *Angewandte Chemie*, 114(18): 3539-3542.
73. Estarellas C, Frontera A, Quiñonero D, Deyà P M. (2011). Relevant anion–π interactions in biological systems: The case of urate oxidase. *Angewandte Chemie*, 123(2): 435-438.
74. Lucas X, Bauzá A, Frontera A, Quinonero D. (2016). A thorough anion–π interaction study in biomolecules: on the importance of cooperativity effects. *Chemical science*, 7(2): 1038-1050.
75. Takamuku S, Nakano M, Kertesz M. (2017). Intramolecular pancake bonding in helical structures. *Chemistry–A European Journal*, 23(31): 7474-7482.
76. Lipinski C A, Lombardo F, Dominy B W, Feeney P J. (1997). Experimental and computational approaches to estimate solubility and permeability in drug discovery and development settings. *Advanced drug delivery reviews*, 23(1-3): 3-25.
77. Montanari F, Ecker G F. (2015). Prediction of drug–ABC-transporter interaction—Recent advances and future challenges. *Advanced drug delivery reviews*, 86: 17-26.
78. Szakács G, Váradi A, Özvegy-Laczka C, Sarkadi B. (2008). The role of ABC transporters in drug absorption, distribution, metabolism, excretion and toxicity (ADME–Tox). *Drug discovery today*, 13(9-10): 379-393.

**How to cite this article:** Mohammad Mazharol Hoque, Ajoy Kumer, Md. Sajib Hussen, Md. Wahab Khan, Theoretical Evaluation of 5, 6-Diaroylisoindoline-1, 3-dione as Potential Carcinogenic Kinase PAK1 Inhibitor: DFT Calculation, Molecular Docking Study and ADMET Prediction. *International Journal of Advanced Biological and Biomedical Research*, 2021, 9(1), 77-104. Link: http://www.ijabbr.com/article_45696.html